From: DYNAMIC LIGHT SCATTERING
Edited by Robert Pecora
(Plenum Publishing Corporation, 1985)

5

Quasielastic Light Scattering from Dilute and Semidilute Polymer Solutions†

D. W. Schaefer

Sandia National Laboratories
Albuquerque, New Mexico 87185

C. C. Han

National Bureau of Standards
Washington, D.C. 20234

5.1. INTRODUCTION

Application of photon correlation spectroscopy (PCS) to polymer dynamics dates back to the inception of the technique in the early 1960s. Early work demonstrated that the self-diffusion constant of large molecules could be obtained by application of PCS to dilute solutions. In addition, some early work dealt with the initial concentration dependence of the diffusion constant. Nevertheless, major advances in the understanding of the dynamics of chain molecules has only occurred in the last few years. In this period there has been a dramatic increase in he amount and significance of PCS activity in polymer physics. The purpose of this review is to summarize and hopefully justify this more recent work.

Two significant factors led to the upsurge of interest by the light scattering community in polymer dynamics. One factor is the application of new theoretical techniques based on scaling methods, renormalization concepts, and linear response techniques to polymer systems. These methods not only brought simple interpretation of known results, but also led to new insights and novel predictions.

† Prepared by Sandia National Laboratories, for the United States Department of Energy under Contract No. DE-AC04-76DP00789

The development of small angle x-ray and neutron techniques has also contributed to the increased interest in polymer physics. These methods are ideally suited to polymers since they are sensitive to spatial dimensions characteristic of chain molecules (100 Å). In addition, neutron scattering coupled with deuterium tagging permits unique experimental measurements such as the properties of a single tagged chain in a matrix of chemically identical untagged chains. Small angle techniques have primarily elucidated static properties since flux problems have precluded quasielastic studies of polymer dynamics. Except for limited experiments based on the newly developed spin-echo technique, PCS has provided the only microscopic probe of polymer dynamics.

The goal of this chapter is not to review the PCS literature but rather to demonstrate how PCS has enhanced understanding of the statistical properties of chain molecules in solution. Since polymer gels, polymer glasses, and phase phenomena are treated elsewhere in this volume, these subjects are not considered. Basic understanding of PCS techniques and polymer fundamentals is assumed. In addition, lengthy derivations are eliminated in favor of ultimate results and interpretation.

For simplicity the single chain problem is treated before adding the complicating effects of interchain interactions and entanglements. The dynamics of a single polymer chain are complex, with many possible approaches to the problem. Therefore, this subject is first treated in a simplified manner employing scaling ideas and later in more detail and rigor using the Zwanzig–Mori formalism. In both cases the renormalization or "blob" concept is introduced to interpret subtle aspects of the molecular wright dependence of the dynamics of a single chain. After the single chain problem, the virial regime is briefly reviewed. The discussion of the virial regime naturally leads to consideration of semidilute solutions. In contrast to the dilute case, the semidilute system is sufficiently complex that a rigorous treatment, even with severe approximations, is not possible. Fortunately, however, dynamical scaling yields results which now seem to be confirmed by PCS measurements in good solvents. Little consideration is given to the concentrated regime since an adequate model is lacking and few experimental data are available.

5.2. THE SINGLE CHAIN

5.2.1. Basic Polymer Statistics

Understanding of the statistical properties of chain molecules centers around two fundamental concepts: the ideal or random-flight chain and

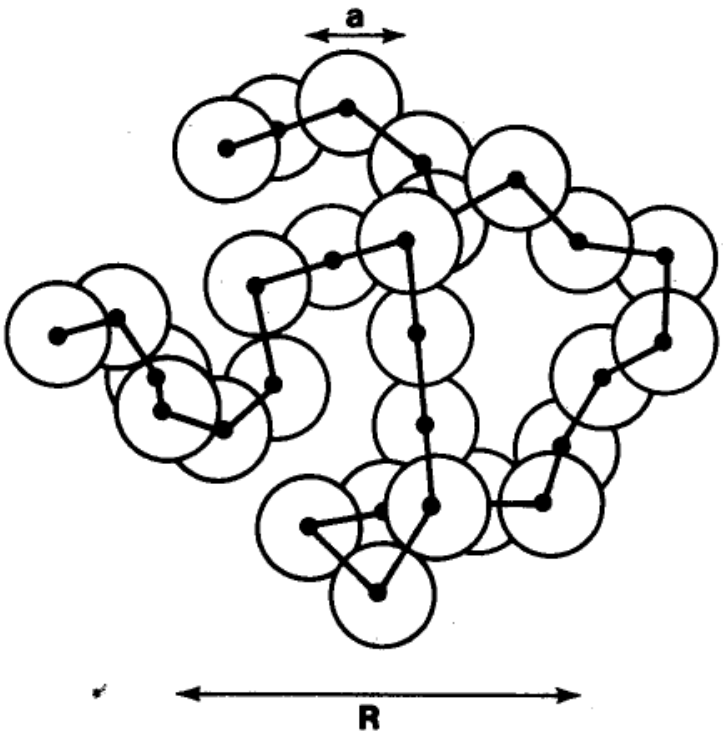

Figure 1. Schematic picture of a polymer. a^3 is the volume associated with a monomer.

chain expansion due to excluded volume. Review of these ideas will lay the groundwork for the discussion of the dynamical properties both in dilute and semidilute solution. The next few sections will attempt to develop a simple and somewhat schematic view of polymers and their dynamical motions.

The simplest model of a polymer is that of a series of connected, noninteracting balls (monomers) of diameter a as illustrated in Figure 1. If the connections between the monomers are stiff universal joints, then the sequence of vectors connecting them defines a random-flight trajectory. In the limit of many joints the radius R of such a sequence is well known[1]

$$R \equiv \langle R^2 \rangle^{1/2} = n^{1/2} a N^{1/2} \tag{1}$$

where N is the number of steps in the sequence or the degree of polymerization, n is a constant, and a is the segment length. The constant n is related to the chain stiffness and can be calculated from the characteristic ratio C_∞ of the chain.[1] At this point it is not necessary to precisely define the radius R, which may be the end-to-end distance, the radius of gyration R_g, or the radius of hydration R_h. These various lengths differ through the factor n. In consideration of dynamic properties R will generally be associated with the hydrodynamic radius R_h. In polymer solutions, ideal or

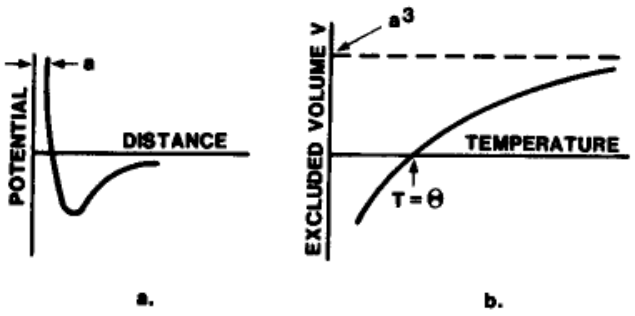

Figure 2. The effective potential between monomers is similar to that between any molecules: repulsive at short range and attractive at larger distances. Figure 2b shows the temperature dependence of the effective interaction between monomers, which is called the excluded volume v. At high temperature, v approaches a^3.

Gaussian behavior described by equation (1), is observed in some cases. The particular temperature at which equation (1) is observed is called the theta temperature ($T = \theta$) and at this point the effective two-body interaction between monomers (excluded volume) vanishes.

Away from the theta point, chains may be swollen or collapsed due to the repulsive or attractive forces between monomers. The forces between monomers are conveniently characterized by an excluded volume v, a concept borrowed from the virial theory of dilute gases.[2] If the temperature is high, monomer interaction is dominated by the repulsive part of the pair potential illustrated in Figure 2a. At high T then the effective excluded volume is just the hard core volume, $v \cong a^3$. At lower temperatures the attractive part of the pair potential dominates and the excluded volume becomes negative, indicative of a net attraction. The point at which $v = 0$, illustrated in Figure 2b, is the theta temperature where the excluded volume or effective two-body interaction vanishes. In this chapter only the regime $v \geq 0$ will be considered. The collapsed state ($v \leq 0$) is intimately connected with phase separation and therefore is not treated here.

The properties of polymers in the swollen state ($T > \theta$) were originally worked out in the mean-field approximation by Flory.[3] Basically, Flory considers the free energy of the chain to consist of an entropic or elastic contribution plus an enthalpic contribution due to the excluded volume interaction. Minimization of the free energy then leads to the so-called Flory law

$$R = a\left(\frac{v}{a^3}\right)^{1/5} n^{1/5} N^{3/5} \tag{2}$$

Although the Flory approach has well-known shortcomings,[4] the 3/5 exponent in the molecular weight dependence of R is well established

experimentally for polymers dissolved in good solvents. Renormalization-group calculations yield an exponent 2% smaller than Flory's calculation, but the difference is beyond experimental resolution at this time.

In solvents of intermediate quality, excluded volume effects are weak and scaling exponents between 1/2 and 3/5 are often observed experimentally. This intermediate regime can be analyzed by perturbation theory,[5] where R is expanded about $T = \theta$ in terms of an expansion factor $Z = va^{-3}N^{1/2}$. Perturbation theory is only expected to be valid near the theta point where v is approximately linear in the temperature increment $\tau = (T - \theta)/T$

$$\frac{v}{a^3} = 1 - 2\chi = (1 - 2\chi_s)\tau, \qquad \tau \ll 1 \tag{3}$$

where the Flory[6] reduced residual chemical potential χ and reduced residual partial-molar entropy χ_s have been introduced. The validity of perturbation theory requires $Z \ll 1$ or $\tau \ll N^{-1/2}$. In addition, the so-called two-parameter perturbation approach also requires that two-body interactions dominate three-body interactions. In virial language this condition becomes

$$v > w\rho \tag{4}$$

where w is the three-body excluded volume or third-virial coefficient. By analogy with simple fluids,[7] $w \sim a^6$ so that condition (4) reduces to $\tau \gg N^{-1/2}$ since the density ρ inside the chain is proportional to $N^{-1/2}$.† Except for unusual circumstances, therefore, it is unlikely to have weak two-body interactions which still dominate three-body effects.

Recently, Farnoux *et al.*[8] developed an interesting alternative to perturbation theory for the intermediate regime. In this so-called "blob" approach short sequences are approximated as ideal ($R \sim N^{1/2}$) whereas long sequences are considered fully swollen ($R \sim N^{3/5}$). In spite of its simplicity, this model has been very successful in explaining both static and dynamic properties of dilute polymers. The blob concept will play a key role in the analysis of chain dynamics which follows.

† The symbol $\sim$ is used to define power-law dependences and does not imply that both sides of the equation have the same dimensions.

5.2.2. Dynamical Regimes

In a photon correlation experiment dynamical information is extracted from the intensity correlation function $\langle I(q, t)I(q, 0)\rangle$, which is directly related to the intermediate scattering function $S(q, t)$

$$\langle I(q, t)I(q, 0)\rangle - \langle I^2\rangle = \beta S^2(q, t), \qquad t > 0 \tag{5a}$$

$$S(q, t) = \frac{1}{V}\sum_{ij} \exp\{i\mathbf{q} \cdot [\mathbf{r}_i(t) - \mathbf{r}_j(0)]\} \tag{5b}$$

where V is the scattering volume, $\mathbf{q}$ is the scattering vector, and $\mathbf{r}_i(t)$ is the position of the monomer i at time t. β is a constant which depends on geometrical factors. Interpretation of light scattering experiments then requires a model for $S(q, t)$ which is consistent with the structure of the polymer and the laws of physics. Since $S(q, t)$ has been calculated exactly only for models with severe approximations, the complete interpretation of scattering experiments is therefore not possible at this time.

Fortunately, considerable progress in the interpretation of PCS experiments can be made on the basis of rather simple arguments. For example, in the limit $qR \ll 1$, $S(q, t)$ is sensitive to fluctuations whose Fourier spatial wavelength q^{-1} is large compared to the size of a single chain. In this regime it follows immediately that the dominant relaxation process is center-of-mass (CM) diffusion. By analogy to hard-sphere systems $S(q, t)$ is exponential with a characteristic decay rate $\Omega = Dq^2$. By contrast, when $1 \ll qR \ll qa$, only internal chain distortions are important and CM diffusion can be neglected. Finally, when $qa \simeq 1$ the motion of single monomers becomes important and the characteristic time of $S(q, t)$ is related to monomer mobility.

5.2.2.1. The Fundamental Relaxation Time. The scaling approach to polymer dynamics rests on the assumption that there is only one fundamental relaxation rate.[9] If the fundamental relaxation rate can be identified then scaling permits characterization of the relaxation processes in dynamical regimes where the fundamental process is no longer dominant. Support for the idea of a single relaxation parameter comes from the static properties of chain molecules. Here a single parameter R_g characterizes the monomer pair distribution function for both ideal and swollen chains. This single characterstic length underlies static scaling methods.

By analogy to the static situation it is reasonable to believe that the fundamental chain relaxation process will dominate when $qR = 1$. That is, the fundamental rate Ω_0 is associated with the fundamental length R. Since $qR = 1$ defines the crossover from CM to internal motion either of these

processes could be used to define Ω_0. From the CM diffusion side, Ω_0 is the rate associated with diffusion over a distance R

$$\Omega_0 = \frac{D}{R^2} \tag{6}$$

Ω_0 could equally well be derived from the tumbling time of a Brownian sphere of radius R

$$\Omega_0 = \frac{kT}{\zeta_{ch} R^2} \tag{7}$$

where ζ_{ch} is the overall chain friction constant. Finally, if there is indeed but one characteristic rate at $qR = 1$ then chain distortions must also display consistent dynamics.

The dynamics of the distortional breathing mode can be established by balance of elastic forces with viscous forces as the chain expands or contracts from its equilibrium distribution.[9] The elastic force can be obtained from linear response theory by imagining that the chain ends are subjected to a fictitious force **f**. Since the energy associated with the resulting distortion $\delta\mathbf{r}$ is $\mathbf{f} \cdot \delta\mathbf{r}$, then the mean distortion is

$$\langle \delta\mathbf{r} \rangle = \frac{1}{Q} \int \delta\mathbf{r} \exp(-\beta H_0 + \mathbf{f} \cdot \delta\mathbf{r}) \tag{8}$$

where Q is the partition function and H_0 is the energy in the absence of f. For small distortions equation (8) can be linearized

$$\langle | \delta\mathbf{r} | \rangle = \frac{R^2}{kT} f \tag{9}$$

Inversion of (9) gives the elastic force associated with a distortion δr. When this force is balanced by the viscous force, we find

$$\frac{kT}{R^2} \langle | \delta\mathbf{r} | \rangle = \zeta_{ch}(\delta\dot{r}) \tag{10}$$

where ζ_{ch} is still the friction constant associated with the entire chain. Equation (10) implies an exponential time correlation function $S(q, t)$ with decay rate equivalent to equation (7). All three possible relaxation pro-

cesses, therefore, give the same relaxation time since (6) and (7) are consistent with the Einstein formula for D

$$D \sim \frac{kT}{\zeta_{ch}} \tag{11}$$

5.2.2.2. Models of Chain Friction. The fundamental relaxation rate Ω_0 depends on the self-diffusion constant D (or equivalently on ζ_{ch}). It is D that contains model specific information. Because of the connectedness of the chain, the motions of the individual monomers are coupled by elastic as well as hydrodynamic interactions. Within certain approximations, however, the coupling can be handled and a simple picture of polymer dynamics emerges.

A reasonable starting point for calculation of D is the Kubo formula[4]

$$D = \frac{kT}{\zeta_{ch}} = \frac{1}{3}\frac{1}{N^2}\int_0^\infty \left\langle \sum_n \mathbf{V}_n(0) \cdot \sum_m \mathbf{V}_m(t) \right\rangle dt \tag{12}$$

where $\mathbf{V}_n(t)$ is the instantaneous velocity of monomer n at time t. The monomer velocities are correlated because the motion of one monomer necessarily leads to a velocity field in the solvent. This solvent motion then leads to a hydrodynamic force which moves other monomers. Solution of equation (12) requires detailed knowledge of the velocity correlations between monomers, and different levels of approximation have been considered to treat this problem.

Within what is known as the Rouse model, hydrodynamic interactions between monomers are completely ignored so that $\langle \mathbf{V}_n(0) \cdot \mathbf{V}_m(t) \rangle = \delta_{nm} \langle \mathbf{V}_n(0) \cdot \mathbf{V}_m(t) \rangle$ and equation (12) reduces to

$$D \cong \frac{D_m}{N} \tag{13}$$

where D_m is the monomer diffusion constant and η is the solvent viscosity,

$$D_m = \frac{kT}{\zeta_m} = \frac{1}{3}\int_0^\infty \langle \mathbf{V}_1(0) \cdot \mathbf{V}_1(t) \rangle \, dt \tag{14}$$

In the Rouse model then

$$\Omega_0 = \frac{D_m}{R^2 N} \tag{15}$$

Although the Rouse model is generally associated with ideal chains, equation (15) depends only on the lack of hydrodynamic interactions and is not dependent on ideal statistics. In spite of the drastic approximations involved in the Rouse model, Rouse-type dynamics may be expected under certain conditions. At extremely short times, for example, $S(q, t)$ may not reflect hydrodynamic interactions due to the finite relaxation time associated with the solvent viscosity. Also, in concentrated solution and melts, where hydrodynamic interactions are screened by other chains, Rouse behavior is expected. The latter case is just now under study by quasielastic neutron scattering.[69]

Solution of equation (12) with hydrodynamic interactions was originally obtained by Kirkwood and Riseman[10] (KR), and their calculation has been summarized in the present context by de Gennes.[4] The central approximation in the KR approach is that temporal and spatial correlations contained in equation (12) are independent so that a given monomer is assumed to feel the average rather than instantaneous flow field of all the other monomers. The result of the KR approach is relatively simple,

$$D = \frac{kT}{6\pi\eta}\left\langle\frac{1}{r}\right\rangle \tag{16}$$

where $\langle 1/r\rangle$ is an average over the static monomer pair correlation function $g(r)$. In the infinite chain limit there is only one length scale and $\langle 1/r\rangle$ is proportional to R^{-1} so that

$$D \sim \frac{kT}{\eta R} \tag{17}$$

and the fundamental relaxation time follows from equation (17)

$$\Omega_0 \sim \frac{kT}{\eta R^3} \tag{18}$$

when equation (18) is specialized to theta conditions ($R \sim N^{1/2}$), the result is generally associated with Zimm,[11] who first calculated the mode structure for the case of an ideal chain with hydrodynamic interactions. Equation (18) is more general, however, and should be valid for swollen chains as well.

The form of equation (18) arises because of the form of the flow field which results from monomer motion. This field, which is described by the Oseen tensor, is long range (decaying as $1/r$) so that monomers substantially removed from each other become hydrodynamically coupled. As a result,

the effective friction constant in the KR approximation is greatly reduced compared to the Rouse case. The particular average in equation (16) is called the hydrodynamic radius R_h,

$$R_h = \left\langle \frac{1}{r} \right\rangle^{-1} \tag{19}$$

5.2.2.3. Scaling[4]. Having established the rate of the fundamental mode at $qR = 1$, it is now possible to proceed to the neighboring limiting regimes using scaling ideas.[12] In particular, for $qR \neq 1$ the relaxation rate is presumed to follow power law behavior,

$$\Omega = \Omega_0 (qR)^x \tag{20}$$

where the exponent x is to be determined. For example, when $qR \ll 1$ then equation (20) should reduce to a diffusional form, i.e., $\Omega \sim q^2$, so that $x = 2$, and using (18),

$$\Omega = Dq^2, \qquad qR \ll 1 \tag{21}$$

as expected. In the opposite limit, $qR \gg 1$, the relaxation processes of interest are distortions internal to the chain so Ω should be independent of R. Therefore, from (18) and (20), $x = 3$ and

$$\Omega \sim \frac{kTq^3}{\eta}, \qquad qa \ll 1 \ll qR \tag{22a}$$

Equation (22a) predicts the q dependence of the relaxation rate for a Zimm chain with hydrodynamic interactions. If the same scaling argument is used for a Rouse chain (no hydrodynamic coupling) one finds

$$\Omega \sim \frac{kTq^4}{\eta} \tag{22b}$$

Some evidence exists for Rouse behavior in melts.[69]

In the limit $qa \cong 1$ a new relaxation process associated with the monomer mobility comes into the problem so that scaling is certain to fail. Nevertheless it is reasonable to expect that monomer translational diffusion will dominate and that

$$\Omega \sim D_m q^2 \tag{23}$$

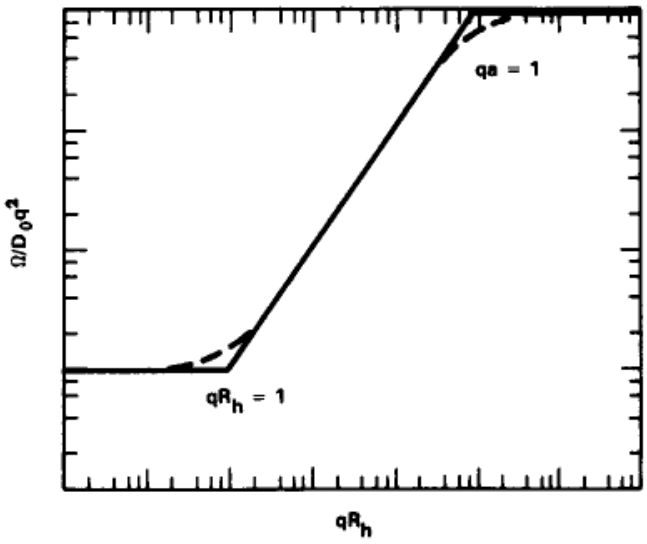

Figure 3. Schematic picture of the normalized relaxation rate $\Omega/D_0 q^2$ associated with $S(q, t)$. Crossover is observed at $qR_h = 1$ and $qa = 1$.

This regime is not accessible by light scattering but is a subject of investigation by quasielastic neutron scattering.[13]

5.2.2.4. Summary and Experimental Data. The above analysis indicates that three dynamical regimes will be observed depending on the value of qR. The three regimes are indicated schematically in Figure 3, where the reduced relaxation rate $\Omega/D_0 q^2$ is plotted versus log qR_h. In the regime $qR_h \ll 1$, $\Omega \sim D_0 q^2$ as expected for center-of-mass diffusion of a chain whose diffusion constant is D_0 at infinite dilution. At $qR_h = 1$, a crossover is observed to the regime where $\Omega \sim q^3$. The crossover is expected to occur at $qR_h = 1$ since R_h is the length scale associated with the fundamental relaxation rate Ω_0. In the regime $qR_h \gg 1$ scaling predicts q^3 dependence regardless of solvent quality. In this intermediate regime $qa \ll 1 \ll qR$, Ω is sensitive to internal dynamics or Rouse–Zimm modes. Finally, when $qa = 1$, a crossover is expected to diffusional motion of individual monomers with monomer diffusion constant D_m.

The general features of Figure 3 are reasonably confirmed by experimental data. Figure 4 shows measured reduced relaxation rates for polystyrene in several solvents ranging from a theta solvent (CH = cyclohexane) to a marginal solvent (EA = ethyl acetate) to good solvents (TOL = toluene, BZ = benzene, and THF = tetrahydrofuran). The mean relaxation rate Ω was obtained from the initial slope of the intensity correlation function defined in equation (5a):

$$\Omega(q) = -\lim_{t \to 0} \frac{d \ln[S(q, t)/S(q, 0)]}{dt} \tag{24a}$$

$$= D_0 q^2, \qquad qR \ll 1, \qquad \phi \to 0 \tag{24b}$$

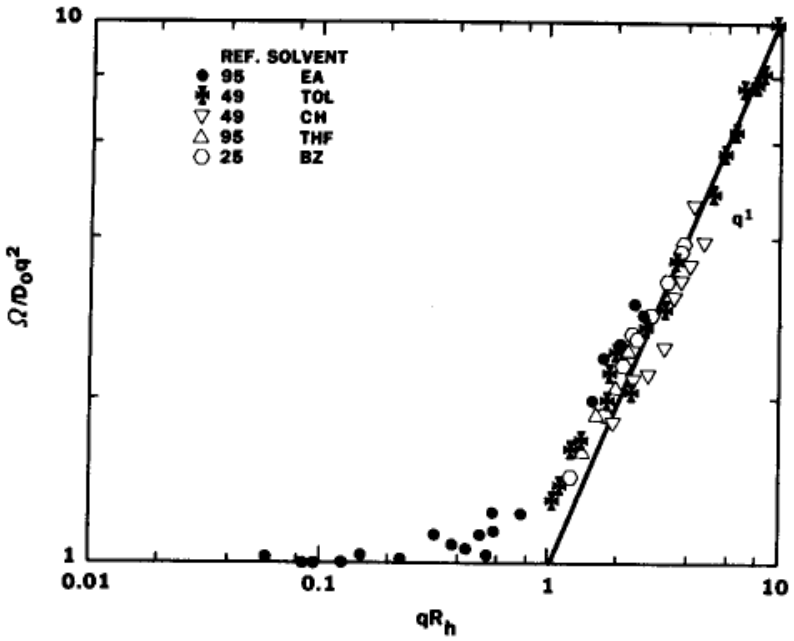

Figure 4. Normalized relaxation rate for PS in several solvents. A universal curve is seen with $\Omega \sim q^3$ in the intermediate region regardless of solvent quality. The log–log plot obscures slight differences in the relaxation rate in theta solvents as opposed to good solvents.

D_0 is the diffusion constant at infinite dilution and ϕ is monomer volume fraction.

The data in Figure 4 demonstrate both the beauty and limitations of the scaling approach. In the regime $qR \ll 1$, diffusional behavior is observed and the relation $\Omega = D_0 q^2$ has been found in many systems. The precise meaning of D_0, however, is not defined by scaling, and in fact questions still exist concerning the dependence of D_0 on the molecular weight. In the following sections a more detailed analysis of D_0 is presented.

Figure 4 shows that the crossover regime spans about one order in q. This crossover regime, which is not subject to scaling analysis, covers many experimental situations. Fortunately, the crossover can be treated by methods outlined in Section 5.2.4.

In the intermediate region, $qa \ll 1 \ll qR$, the data are consistent with scaling predictions, namely, $\Omega \sim q^3$. The scatter in the data, however, obscures any differences which might exist between the data sets in theta vs. good solvents. In fact, slight differences are predicted by linear response theory and these differences are analyzed in more detail in Section 5.2.4.

The high-q regime, where monomer diffusion dominates, is not subject to study by light scattering since the conditions $qa \simeq 1$ cannot be realized. Nevertheless, some results from quasielastic neutron scattering are available, and these data are consistent with the existence of crossover to $\Omega \sim D_m q^2$ at high q. Figure 5 shows data of Nicholson *et al.*[13] taken by

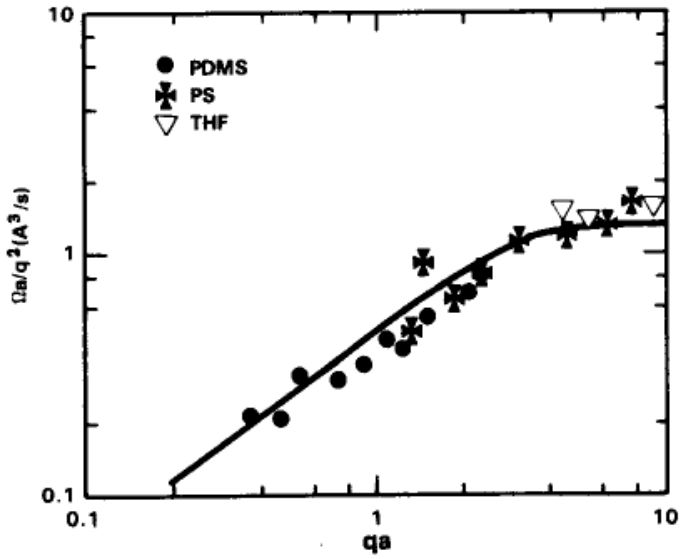

Figure 5. Normalized relaxation rate in the regime $qa \simeq 1$. These quasielastic neutron data[13] are consistent with a crossover to diffusive behavior near $qa = 1$. For $qa > 1$, the relaxation rate is diffusive, the diffusion constant being that of monomer or segment.

neutron spin-echo techniques. The line in the figure is calculated on the basis of the theory outlined in the following section. These data suggest a crossover to q^2 behavior at high q, but they are certainly not definitive.

5.2.3. Center-of-Mass Diffusion ($qR \ll 1$)

Almost all photon correlation experiments performed to date in dilute solution have investigated the regime $qR \ll 1$ where the decay constant Ω is proportional to the diffusion constant D of the chain, equation (21). The profusion of diffusional data is due to the relatively long wavelength of visible light as well as the difficulty of preparing very high molecular weight chains. In theta systems, interpretation of D_0 (D at infinite dilution) is relatively straightforward since D_0 is inversely proportional to the hydrodynamic radius $R_h = \langle r^{-1} \rangle^{-1} \sim D^{-1}$, which in turn scales as $N^{1/2}$ by equation (1). In better solvents, however, interpretation of D_0 is not trivial since D_0 is found to scale with molecular weight to a power intermediate between the ideal value of 1/2 and the Flory exponent 3/5 [equation (2)]. Much of the rest of this section is devoted to an analysis of these intermediate exponents in terms of the so-called "Blob" model, which is a simple conceptualization of the renormalization concept as applied to polymers.

5.2.3.1. Theta Systems. The first systematic study of D_0 in theta systems by PCS is the work of King *et al.*[14] on polystyrene (PS) in cyclohexane (CH). The molecular weight dependence of D_0 for PS in CH at the theta temperature is shown in Figure 6. Equation (17) suggests that D_0

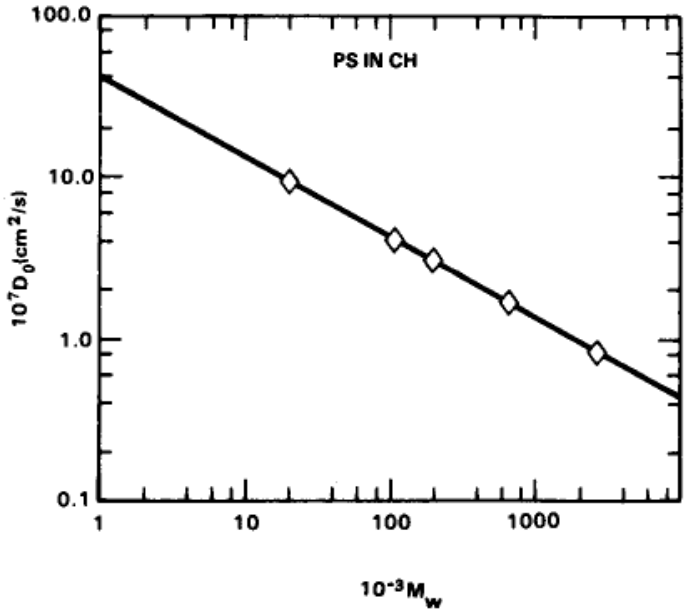

Figure 6. Molecular weight dependence of the diffusion constant in dilute theta solution.[14] D_0 is obtained from the relaxation rate of $S(q, t)$ at $qR \ll 1$ and infinite dilution. The line is of slope $-1/2$ as expected for an ideal chain. $T = 35°C$, PS in cyclohexane.

should scale as $N^{-1/2}$ in this system since the chains are ideal. The line in Figure 6 shows this power law dependence.

5.2.3.2. Marginal and Good Solvents. (a) *Molecular Weight Dependence.* In good solvents, when the chains are highly swollen, both scaling arguments and linear response theory predict $\Omega \sim \langle r^{-1} \rangle \sim N^{-\nu_h}$, where $\nu_h \cong 3/5$ is the Flory exponent. All recent light scattering experiments, however, show weaker power law dependence. Table 1 summarizes the measured exponents ν_h found for polystyrene (PS) and poly-α-methyl styrene (PAMS) in several solvents. A reasonable explanation[15, 16] for the anomalous exponents is that the hydrodynamic radius $R_h = \langle r^{-1} \rangle$ is sensitive to short sequences within the chain and therefore R_H does not reach its asymptotic limit ($N \to \infty$) within the range of experimental values of the molecular weight.

It has been known for many years that short chains and short sequences within chains show less swelling than longer chains.[3] This scale dependence of swelling coupled with the sensitivity of Ω to short distances explains the observed intermediate exponents. Basically the probability of intrachain contact increases with molecular weight so short chains with few intrachain contacts are nearly ideal.

The ideality of short sequences can be crudely modeled by considering the chain to be a sequence of "blobs" or renormalized monomers as shown

Table 1. Parameters for Polymer Systems[a]

System	T (°C)	Θ (°K)	τ	$10^2\eta$	ν_h	L (Å)	N_τ	χ_{pcs}	χ	χ_s
PS in										
CH[14]	35	307[6]	0	0.762	0.491	8.19	—	0.5	0.5[6]	0.2[6]
EA[22]	25	229[28]	0.232	0.426	0.515	8.66	2620	0.480	0.49[3]	0.47[6]
MEK[21]	25	0[6]	1	0.38	0.525	8.78	656	0.458	0.494[6]	0.50[6]
BZ[25]	20	(100)[6]	0.66)	0.649	0.537	9.73	482	0.451	0.44[3]	0.41[3]
THF[23, 68, 87]	25	—	—	0.46	0.559	10.13	80.0	0.379	—	—
TOL[24, 86]	20	(160)[6]	(0.46)	0.589	0.567	8.03	49.8	0.347	0.36[71]	0.39[3]
EBZ	25	—	—	—	—	—	—	—	0.40[6]	0.42[6]
PAMS in										
TOL[27]	25	—	—	0.552	0.534	7.92	193	0.411	0.36[70]	—
BZ[27]	30	—	—	0.561	0.536	7.87	163	0.403	—	—
PDMS in										
TOL	20	—	—	—	—	—	—	—	0.43[89]	—

[a] T is the temperature at which diffusion measurements were made. In some cases different temperatures were reduced to a common temperature, assuming $D_0 \sim T/\eta$. η is the viscosity used in fitting D_0 vs. M to equation (27) with L and N_τ being the parameters resulting from such a fit. X_{pcs} is calculated using equation (25b), assuming $n = 1.67$ for PS and $n = 1.84$ for PAMS. v_h is the apparent hydrodynamic exponent found from the slope of log D_0 vs. log M. τ is calculated using equation (68). Numbers in parentheses are very approximate.

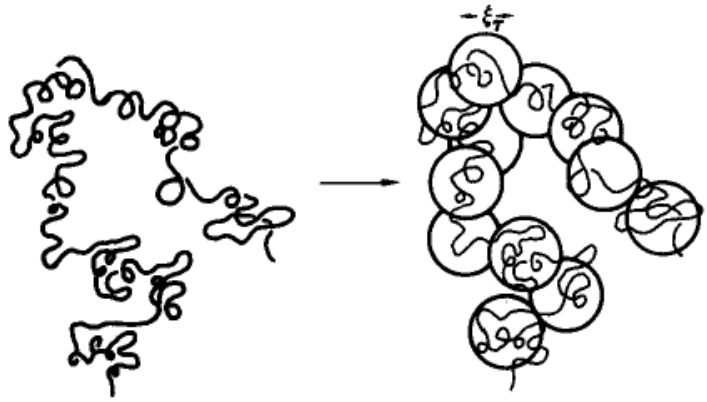

Figure 7. A schematic picture of the thermal blob model of polymers.[8] The actual chain on the left is divided into blobs on the right whose temperature-dependent radius ξ_τ is the mean distance smaller than the radius at which the chain is ideal. Inside the blob the chain is assumed to be ideal, whereas the renormalized chain, consisting of a sequence of blobs of radius ξ_τ, is swollen due to excluded volume. The blob model correctly predicts many polymer properties but it is a drastic oversimplification.[17] Most global properties are not strongly affected, however, by correcting[18] the deficiencies of the blob model.

in Figure 7. The actual chain on the left is divided into a sequence of blobs of radius ξ_τ. Within the blob the chain is ideal so that

$$\xi_\tau = (nN_\tau)^{1/2}a \tag{25a}$$

where N_τ is the temperature-dependent cutoff for ideal behavior. N_τ can be obtained by equating equations (1) and (2) with the result [$v = a^3(1 - 2\chi)$]

$$N_\tau = \frac{n^3}{(1 - 2\chi)^2} \tag{25b}$$

The renormalized chain or sequence of blobs shows swelling so that by analogy with equation (2)

$$R \sim \left(\frac{N}{N_\tau}\right)^{3/5} \xi_\tau \tag{26}$$

A qualitative explanation for the intermediate exponents ν_h in Table 1 follows from equations (25) and (26). That is, since D_0 is proportional to the first reciprocal moment of the monomer pair distribution function, it is sensitive to sequences short compared to ξ_τ. Since short sequences are nearly ideal, exponents closer to 1/2 than 3/5 are reasonable even in relatively good solvents where the radius of gyration R_g scales with molecular weight dependence near $N^{3/5}$.

Akcasu and Han[16] have worked out a detailed expression for D_0

within the blob model. Their result depends on $x = N_\tau/N$, the ratio of the chain to the blob molecular weight

$$D_0 = \frac{kT}{6\pi\eta}\frac{1}{LN^{1/2}}\frac{12}{(6\pi)^{1/2}}x^{1/2}2\left(1-\frac{x}{3}\right) + \frac{1}{1-\nu}(x^{\nu-1}-1) - \frac{1}{2-\nu}(x^{\nu-1}-x) \quad (27)$$

where $L \simeq na$ is an unknown length scale which is equal to a for a completely flexible chain. Equation (27) shows the expected crossover from ideal to swollen behavior as x increases:

$$D_0 = \frac{kT}{6\pi\eta L}\frac{12}{(6\pi)^{1/2}}\frac{1}{(1-\nu)(2-\nu)N^{\nu}} \sim N^{-\nu}, \qquad x \ll 1 \quad (28)$$

$$D_0 = \frac{kT}{6\pi\eta L}\frac{16}{(6\pi)^{1/2}N^{1/2}} \sim N^{-1/2}, \qquad x = 1 \quad (29)$$

Figures 8–12 show the existing literature data for the molecular weight dependence of the diffusion constant of PS in various solvents. In all cases the line is a best fit to the data using equation (27) with L and N_τ as

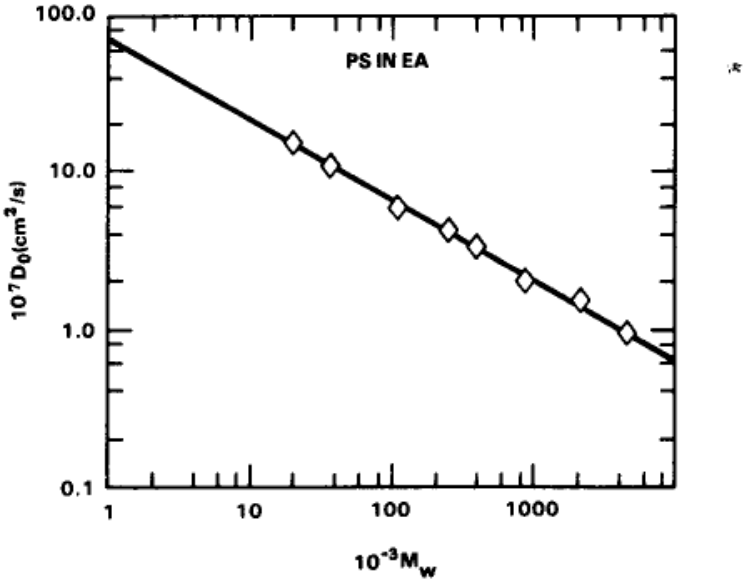

Figure 8. Molecular weight dependence of D_0 for PS in ethyl acetate[22] which is a near theta solvent. The line is a fit to equation (27) with L and N_τ as parameters. These parameters are listed in Table 1. For this system, $N_\tau \cong 2600$, which means a sequence must contain 2600 monomers before showing appreciable swelling due to excluded volume interactions. $T = 25°C$.

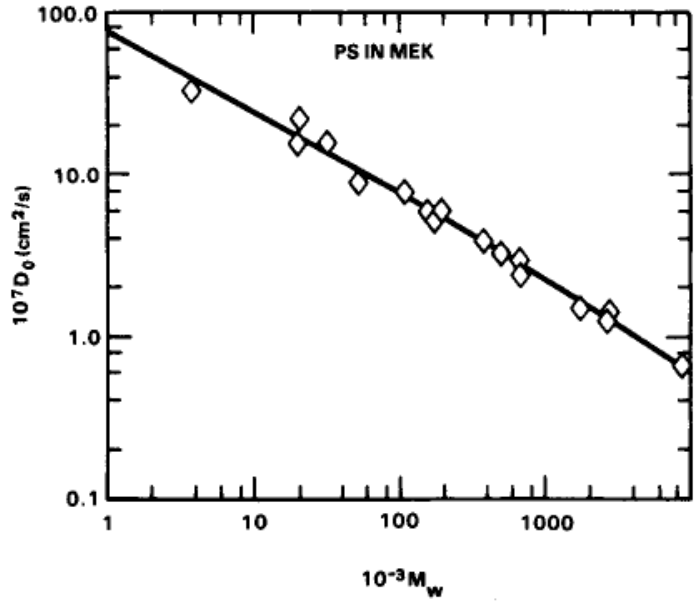

Figure 9. Molecular weight dependence of D_0 for PS in methyl ethyl ketone,[21] a marginal solvent. $T \simeq 25°C$.

parameters. The values of these parameters are collected in Table 1 for these data and others for poly-α-methyl styrene (PAMS).[27] Examination of N_τ in Table 1 indicates that N_τ is a measure of solvent quality. For good solvents such as THF and TOL, N_τ is of the order of 100 monomers whereas for marginal solvents such as EA, $N_\tau \sim 10^3$. Increasing N_τ correlates directly with decreasing values of the apparent exponent ν_h. The Flory

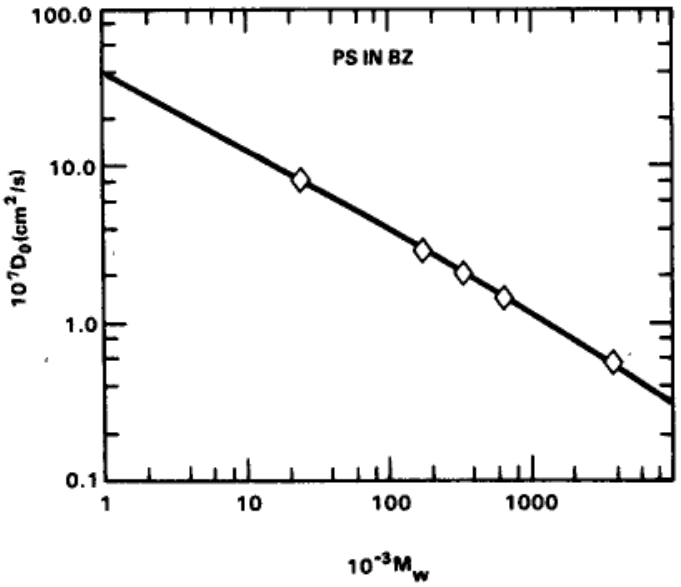

Figure 10. Molecular weight dependence of D_0 for PS in benzene.[26] Benzene is probably best classified as a marginal solvent. $T = 20°C$.

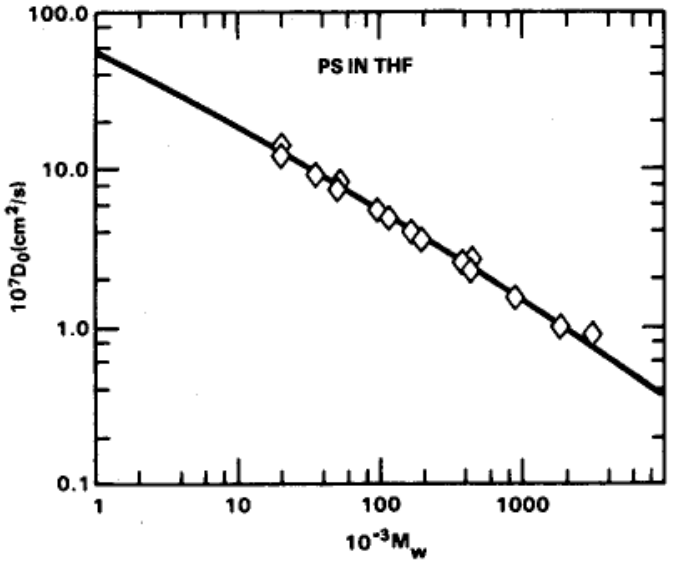

Figure 11. Molecular weight dependence of D_0 for PS in THF.[23, 68, 87] The data are plotted for $T = 25°C$. Data of References 68 and 87 have been reduced to 25°C assuming $D \sim T/\eta$.

reduced residual free energy χ can be calculated from N_τ using equation (25b) and the results are shown in Table 1 as χ_{pcs}. For comparison, χ measured by other means is also shown and the agreement is surprisingly good.

The blob model is known to be a drastic oversimplification since short sequences can deviate substantially from ideality.[17, 18] Nevertheless, the blob concept provides a simple framework to understand polymer statistics

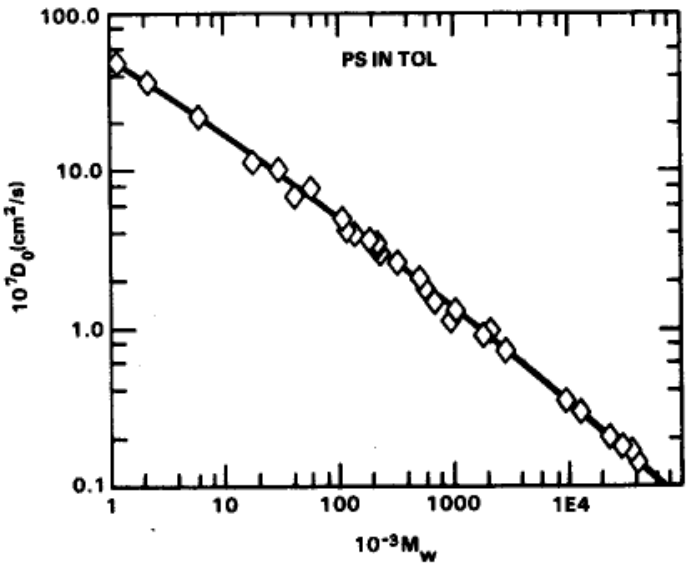

Figure 12. Molecular weight dependence of D_0 for PS in toluene. Toluene is a good solvent so the data approached a slope of $-3/5$ at high molecular weight.

in the intermediate molecular weight range. In this regime no completely satisfactory theory is available.

(b) *Temperature Dependence.* The temperature dependence of chain swelling can also be treated within the blob model. Unfortunately there is very little experimental data on the temperature dependence of the hydrodynamic radius, probably because most organic solvents boil at a relatively low temperature.

The temperature dependence of D_0 follows from equation (27) if the temperature dependence of N_τ is known. Near $\tau = \theta$ the excluded volume is expected to be approximately linear in the temperature increment $\tau = (T - \theta)/T$, so that

$$N_\tau \sim \left(\frac{a^3}{v}\right)^2 n^3 \sim \frac{n^3}{(1 - 2\chi_s)^2 \tau^2} \tag{30}$$

assuming n is temperature independent. Unfortunately, existing data are insufficient to confirm this temperature dependence for N_τ.[16]

5.2.4. Internal Dynamics and the Dynamic Structure Factor

5.2.4.1. Preliminary Considerations. The scaling analysis outlined in Section 5.2.2.3 shows that the basic form of the dynamic structure factor can be obtained by simple scaling analysis. In particular, three regimes separated by $qR_h = 1$ and $qa = 1$ were identified and the functional dependence of the relaxation rate on temperature, molecular weight, viscosity, and q were established. In spite of the success of this analysis, many shortcomings are present in the scaling approach. In the present section, more detailed analysis of $S(q, t)$ is reviewed for several models of chain molecules. This analysis both justifies the scaling approach and fills in details which cannot be obtained by scaling.

The limitations of scaling analysis include the following problems. First, no underlying justification for scaling or power laws was given. Second, the shape of $S(q, t)$ and the relationship between the characteristic frequency Ω and $S(q, t)$ is not obvious. In addition, scaling yields power law exponents but not coefficients. Information on chain statistics and monomer interactions is available from coefficients as shown below. Finally, scaling does not treat the transition regions $qa = 1$ and $qR = 1$. These regions are important experimentally and fortunately $S(q, t)$ is available in the crossover regimes for certain simplified models of polymer chains.

Ideally, interpretation of dynamic scattering experiments requires a

theory that can predict $S(q, t)$ under actual experimental conditions which are characterized by temperature, concentration, and a chain model consistent with the chemical structure of the polymer. Unfortunately, exact expressions for $S(q, t)$ are available at present only for a single unperturbed (Θ-condition) Gaussian chain without hydrodynamic interaction (Rouse model), and in the infinite chain limit, with hydrodynamic interaction and preaveraged Oseen tensor (Rouse–Zimm model). In this sense, a complete interpretation of dynamic scattering experiments on polymer solutions is an unsolved problem. Nevertheless the interpretation of scattering experiments can proceed in terms of the initial slope $\Omega(q)$ of the normalized intermediate scattering function $S(q, t)$. The initial slope is defined by equation (24a) and should reduce to q^2D as $q \to 0$. $\Omega(q)$ turns out to be identical to the relaxation rate Ω which was derived by scaling analysis in Section 5.2.2.3. By using linear response theory, $\Omega(q)$ can be calculated for many different models. For example, $\Omega(q)$ as a function of temperature and concentration has been calculated in terms of the "blob" model.[19]

No attempt will be made in this section to derive $S(q, t)$ and $\Omega(q)$ for the various models. Rather, the results of these various calculations will be analyzed graphically to demonstrate the effect of various experimental parameters such as hydrodynamic coupling, monomer excluded volume, temperature, and momentum transfer q. Ideally one should start with a theory for $S(q, t)$ which somehow incorporates hydrodynamic coupling and a temperature-dependent distribution function in a form which does not require approximations such as preaveraging of the Oseen tenor, moment expansions, or asymptotic limits. Unfortunately, such a theory is not available so it is necessary to resort to various levels of approximation to study the influence of various factors on the dynamics.

Table 2 lists the models which are currently available with the appropriate theoretical and experimental references. Akcasu, Benmouna, and Han[20] have treated most of these models starting from a general formalism based on the eigenfunction method and linear response theory. For this review only selected models are discussed to illustrate trends. For example, the q dependence of $S(q, t)$ is analyzed for a Rouse–Zimm ring (model 3) which is the only realistic model for which $S(q, t)$ is available for $qR_g \sim 1$. Data on polystyrene in cyclohexane and toluene are compared with this theory. The dependence of $S(q, t)$ on hydrodynamic coupling is analyzed using models 1 and 4 which are valid only for $qR \gg 1$. The effects of excluded volume and hydrodynamic preaveraging are discussed only with respect to the characteristic frequency $\Omega(q)$ since full calculations of $S(q, t)$ are not available. In all cases, comparison with experimental data is shown when data are available.

In 1965, Pecora showed[29] for the first time that the intermediate

Table 2. Models for Chain Dynamics

Name, model	Function calculated	Regime	Statistics	Hydrodynamics	Monomer interaction	Geometry	Refs.
1. Rouse	S, Ω	All	Gaussian	None	None	Linear	20, 29, 30
2. Rouse	S, Ω	All	Gaussian	None	None	Ring	20
3. Rouse–Zimm ring	S, Ω	All	Gaussian	Preav.	None	Ring	20
4. Rouse–Zimm ∞ chain	S, Ω	$KR_g \gg 1$	Gaussian	Preav.	None	Ring or linear	20, 31, 32, 34
5. (unnamed)	Ω	All	Quasi-Gaussian	Preav.	Blob approx.	Linear	19, 34
6. (unnamed)	Ω	All	Quasi-Gaussian	Nonpreav.	Blob approx.	Linear	19, 34
7. (unnamed)	Ω	All	Gaussian	Nonpreav.	None	Ring	40
8. Freely jointed chain	Ω	All	Freely jointed	Preav.	None	Linear	41
9. Sliding rod	Ω	All	Sliding rod	Preav.	None	Linear	42
10. Harris–Herst	Ω	All	Wormlike	Preav.	None	Linear	44

scattering function $S(q, t)$ for a flexible polymer chain can be calculated by using a Green's function solution of the Fokker–Plank equation for the bead-and-spring model. Later, de Gennes and Debois-Violette[30, 31] calculated $S(q, t)$ in the intermediate q region, that is, for $qR_g \gg 1 \gg qa$, where R_g is the radius of gyration of the polymer and a is the segment length of the polymer. They demonstrated the q^3 and q^4 dependence of relaxation rate in the cases with and without hydrodynamic interaction for a Gaussian chain. They also showed that $S(q, t)$ will follow a universal shape in this intermediate region if time is scaled by a characteristic frequency.

If one follows the approach of Zwanzig and Fixman[20, 32–34] by assuming that the distribution function, ψ, of the monomers is a function which satisfies a dynamical equation

$$\frac{\partial \psi}{\partial t} = D\psi \tag{31}$$

with D as a linear, time-independent diffusion operator, then, one can define a self-adjoint operator $\mathscr{L}$ through

$$D(\psi A) \equiv -\psi \mathscr{L} A \tag{32}$$

where A is an arbitrary dynamical variable such as Fourier transform of the monomer density $\rho(q, t) \equiv \sum_j e^{iq \cdot R_j}$.

The intermediate scattering function can be written as

$$\begin{aligned} S(q, t) &= \langle \rho(q, 0)\rho(q, t) \rangle \\ &\equiv \langle \rho, e^{-t\mathscr{L}} \rho \rangle \\ &\equiv \langle \rho, \rho(t) \rangle \end{aligned} \tag{33}$$

For an eigenvalue problem[5, 35]

$$\mathscr{L} v_n = \omega_n v_n \tag{34}$$

Equation (33) can be written as

$$\begin{aligned} S(q, t) &= \sum_n \langle \rho, v_n \rangle \langle v_n, e^{-t\mathscr{L}} \rho \rangle \\ &= \sum_n e^{-\omega_n t} |\langle v_n, \rho \rangle|^2 \end{aligned} \tag{35}$$

Also the characteristic frequency $\Omega(q)$ can be obtained through differentiation as

$$\Omega(q) = \sum_n \omega_n |\langle v_n, \rho \rangle|^2 / S(q, 0)$$
$$= \langle \rho, \mathscr{L}\rho \rangle / \langle \rho, \rho \rangle \tag{36}$$

Whenever a model polymer can be solved as an eigenvalue problem, *in principle* the corresponding scattering problem is solved. This principle can be seen from cases 1 through 4 in Table 2.

In the case in which $S(q, t)$ cannot be solved, progress may still be possible through the calculation of the characteristic frequency $\Omega(q)$. This procedure is discussed later. One should observe from equation (36) that the initial slope of $S(q, t)$ or characteristic frequency $\Omega(q)$ is actually a weighted average of all the relaxation times (or eigenvalues). $S(q, t)$ always decays exponentially at short time, but this short-time decay rate, which is the characteristic frequency $\Omega(q)$, bears no simple relationship with the shortest or longest (terminal) relaxation times.

5.2.4.2. Intermediate Scattering Function, $S(q, t)$. (*a*) *q dependence.* In the generalized Kirkwood diffusion equation,[36] a linear flexible polymer is approximated by a bead-and-spring model. All forces are concentrated on these beads. The frictional force on the jth bead is

$$f = -\zeta(v_j - v_j') \tag{37}$$

where ζ is the frictional coefficient, v_j is the velocity of the jth bead, and v_j' is the velocity of the solvent at the jth bead's position produced by all other beads through hydrodynamic interaction which is again approximated by the Oseen tensor as

$$v_j' = \sum_l T_{jl}\zeta(v_l - v_l') \tag{38}$$

with

$$T_{jl} = \frac{1}{8\pi\eta}\left(\frac{1}{R_{jl}^3}\right)[R_{jl}^2\mathbf{1} + \mathbf{R}_{jl} : \mathbf{R}_{jl}]$$

and $T_{jj} = 0$. $\zeta(V_l - V_l')$ is the force exerted on the fluid by the lth bead.

The eigenvalues have been calculated by B. Zimm[11] in 1956 for a preaveraged Oseen tensor. The corresponding case with no hydrodynamic interaction was solved in 1953 by Rouse.[37] In the ring polymer case,[5, 38, 39] because of the cyclic boundary condition, both cases with and without hydrodynamic interactions can be calculated analytically at any chain length N [see Equations (17)–(72) of Reference 20].

Figure 13 shows the variation of $S(q, t)$ as a function of $\Omega(q)t$. For a ring polymer the initial slopes of all curves are equal to -1. It is observed that the shape function tends to a straight line when $qR_g \leq 0.87$ or $qa \geq 10$. The curves also cluster around the curve corresponding to $qa = 1.5$ when

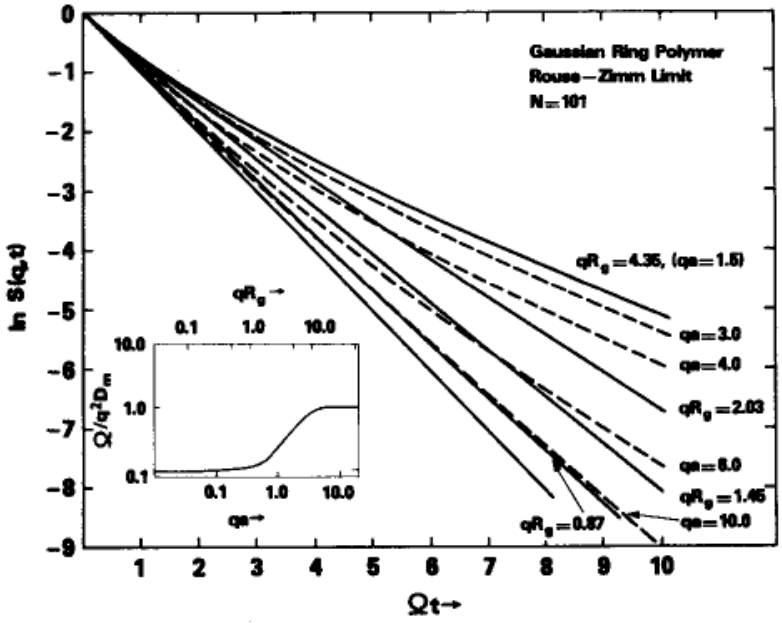

Figure 13. The variation of the shape function ln $S(q, t)$ with normalized time Ωt for various values of q in the presence of hydrodynamic interaction ($B = 0.38$). Also shown is the variation of the initial slope $\Omega(q)$ with (qa).

$qR_g \gg 1$ but $qa \leq 2$. These tendencies become more apparent as N increases. At the same time, the characteristic frequency $\Omega(q)$ approaches a q^3 dependence (see insert of Figure 13).

Since the open and closed chains are identical as chain length $N \to \infty$, the normalized intermediate scattering function $S(q, t)$ with preaveraged Oseen tensor can be found in this limit as

$$S(q, t) = \left(e^{-\alpha\phi_0(t)} + 2\sum_{s=1}^{\infty} e^{-\alpha\phi_s(t)}\right)\left(1 + 2\sum_{s=1}^{\infty} e^{-\alpha s}\right)^{-1} \tag{39}$$

where

$$\phi_s(t) \equiv s + \frac{1}{2\pi}\int_{-\pi}^{\pi} dp\, \frac{1 - \exp(-\alpha_p t)}{1 - \cos p} \cos ps$$

$$\alpha_p \equiv 2W(1 - \cos p)[1 + 2BZ(p)]$$

$$Z(p) \equiv \sum_{n=1}^{\infty} \frac{\cos pn}{(n)^{1/2}}$$

$$\alpha \equiv \frac{q^2a^2}{6}$$

$$W \equiv \left(\frac{3}{a^2}\right) D_m$$

where B is the draining parameter defined below.

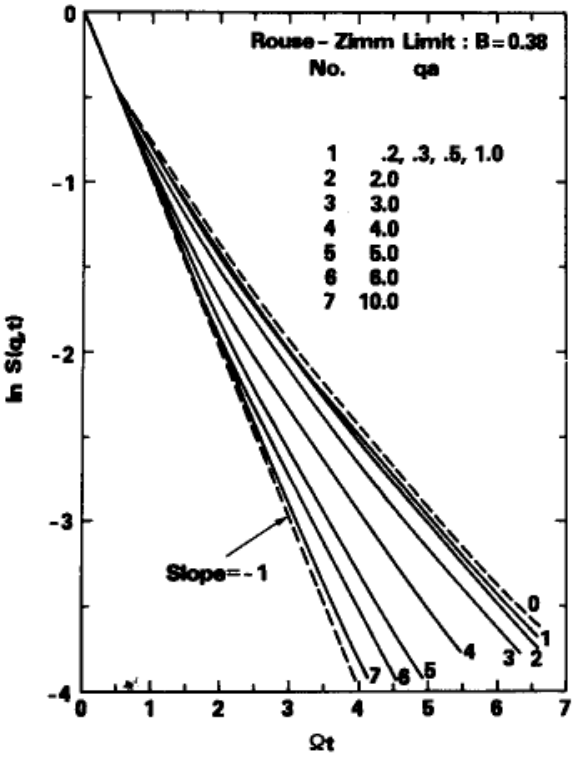

Figure 14. The variation of the shape function ln $S(q, t)$ with normalized time Ωt for various values of qa in the case of an infinite chain with hydrodynamic interaction.

In Figure 14, $S(q, t)$ at various qa values is plotted for the Rouse–Zimm case. In the Rouse case, $S(q, t)$ can be recovered from equation (39) by letting $B = 0$. The Rouse case is displayed in Figure 15 for various qa values.

The form of the normalized $S(q, t)$ in the intermediate q region where $qa \ll 1$ and $qR_g \gg 1$ can be obtained from equation (39) in the limit of $qa \to 0$. The $qR_g \gg 1$ has already been taken into account through $N \to \infty$. The general expression is

$$S(q, t) = \int_0^\infty du \exp\left[-u - J\left(u, \Omega t, \frac{B}{\sqrt{\alpha}}\right)\right] \tag{40a}$$

where

$$J\left(u, Qt, \frac{B}{\sqrt{\alpha}}\right) \equiv \frac{2}{\pi}\int_0^\infty dx \frac{\cos xu}{x^2} \times \left\{1 - \exp\left[-(\Omega t)x^2 \frac{1 + B(2\pi/x\alpha)^{1/2}}{1 + 2B(\pi/\alpha)^{1/2}}\right]\right\} \tag{40b}$$

With

$$\Omega(q) = \frac{1}{12}\left(\frac{kT}{\zeta}\right)q^4a^2\left[1 + \left(\frac{2\sqrt{\pi}\,B}{\sqrt{\alpha}}\right)\right] \tag{41}$$

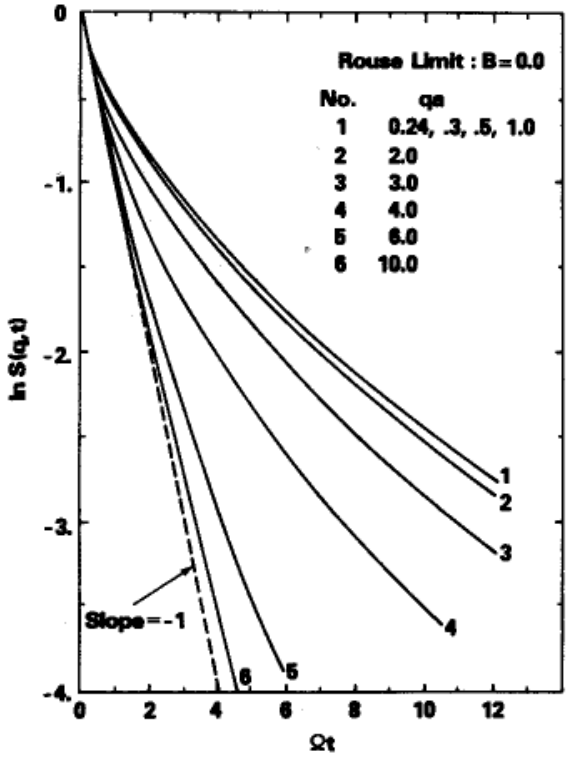

Figure 15. Variation of the shape function ln $S(q, t)$ with normalized time, Ωt, for a Rouse chain.

where B is the draining parameter

$$B \equiv \frac{\zeta/\eta a}{\pi\sqrt{6\pi}} \tag{42}$$

The Rouse model is recaptured with $B = 0$ as

$$S(q, t) = \int_0^\infty du \exp\left\{-u - (\Omega t)^{1/2} g\left[\frac{u}{(\Omega t)^{1/2}}\right]\right\} \tag{43a}$$

where

$$g(u) \equiv \frac{2}{\pi} \int_0^\infty dx \frac{\cos xu}{x^2} [1 - \exp(-x^2)] \tag{43b}$$

and the characteristic frequency

$$\Omega(q) \equiv \frac{1}{12}\left(\frac{kT}{\zeta}\right) q^4 a^2 \tag{44}$$

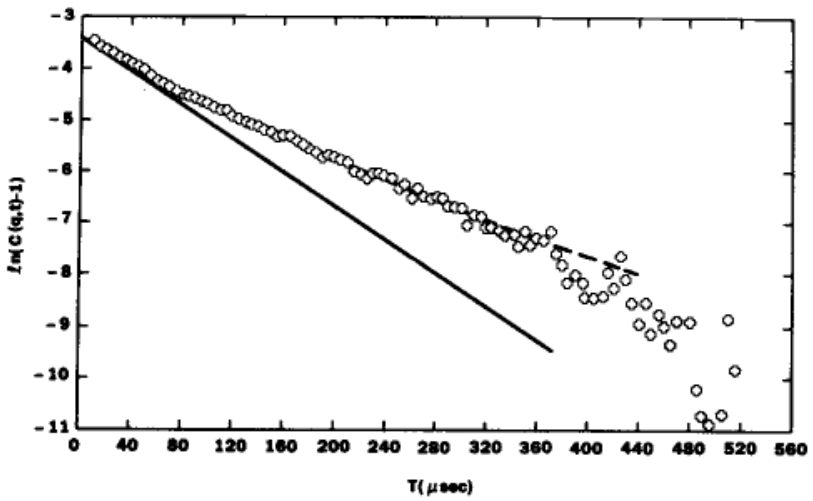

Figure 16. Experimental correlation data of PS ($M_w = 44 \times 10^6$) in cyclohexane at a scattering angle $\theta = 120°$ with a delay time of 5 μsec. The dashed curve is the best fit using the asymptotic shape function, and the solid line is the corresponding initial slope. $T = 35°C$.

On the other hand, the Rouse–Zimm limit can be reached as $qa \ll 2B(6\pi)^{1/2}$ as

$$S(q, t) = \int_0^\infty du \exp\{-u - (Qt)^{2/3} h[u(Qt)^{-2/3}]\} \tag{45a}$$

where

$$h(u) \equiv \frac{2}{\pi} \int_0^\infty dx \frac{\cos xu}{x^2} \left[1 - \exp\left(\frac{-x^{3/2}}{\sqrt{2}}\right)\right] \tag{45b}$$

The initial slope follows as:

$$\Omega(q) = \frac{1}{6\pi} \left(\frac{kT}{\eta}\right) q^3 \tag{46}$$

The following points should be noticed:

(i) $S(q, t)$ is expressed in the intermediate q region as a function of a single variable, $\Omega(q)t$, which combines both q and t. When time is scaled as $\tau = \Omega(q)t$, a universal curve as a function of τ, is obtained for all q values in this q region. This conclusion justifies the interpretation of $\Omega(q)$ as a "characteristic frequency" in the sense of dynamic scaling.

(ii) $\Omega(q)$ is the initial slope of $S(q, t)$ at $t = 0$.

(iii) The q dependence of $\Omega(q)$ follows a power law in the intermediate q region.

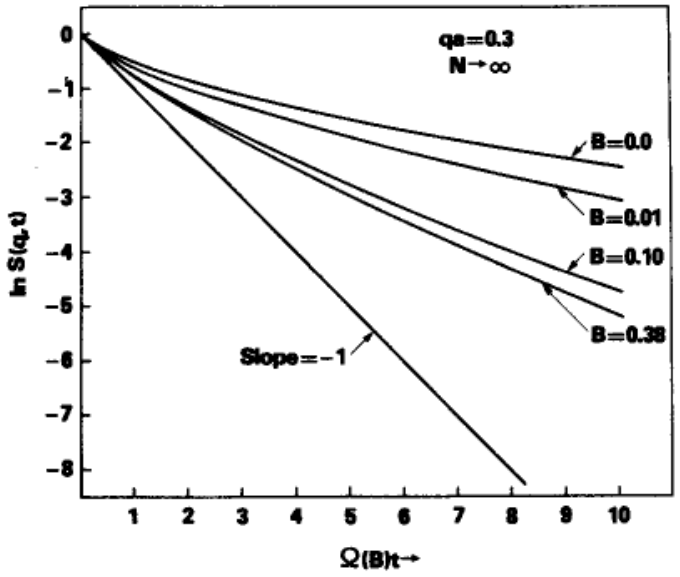

Figure 17. The effect of the draining parameter B on the shape function ln $S(q, t)$.

(iv) For large times $S(q, t) \rightarrow \exp[-(2/\sqrt{\pi})(\Omega t)^{1/2}]$ in the Rouse case and $S(q, t) \rightarrow \exp[-1.35(\Omega t)^{2/3}]$ in the Rouse–Zimm case, although this asymptotic region may not be reached in the realistic experimental time range, i.e., $\Omega t \leq 10$.

In Figure 16, experimental data of $\ln[C(q, t) - 1] = \ln[\beta S^2(q, t)]$ for polystyrene with molecular weight of 44×10^6, $c = 0.11$ mg/ml, and $q = 3.2 \times 10^5$ cm^{-1} is plotted vs. time to demonstrate the asymptotic shape function. Here $C(q, t) = \langle I(q, t)I(q, 0)\rangle/\langle I^2\rangle$ is defined in equation (5). The dotted line is the best fit to equation (45). The solid line is the initial slope of the asymptotic function fit. It is clear that the experimental range is controlled by the signal-to-noise ratio at large times. In this case, correlation data are truncated at 400 μsec in the analysis.

Hydrodynamic Interaction Strength. The notation $B \equiv \zeta_0/\eta a\pi\sqrt{6\pi}$ is used to represent the hydrodynamic interaction strength. It should be noted that in order to keep the dynamical operator as positive definite and avoid degeneracy, B has to be smaller than ~ 0.6.[20, 46–48] In Figure 17, the asymptotic shape function is plotted with several B values to demonstrate the change from the Rouse–Zimm limit (a Flory value of $B = 0.38$ is used[1]) to Rouse limit of $B = 0$.

In general, the effect of B on the shape of $S(q, \Omega t)$ is such that $S(q, \Omega t)$ increases with decreasing B at fixed Ωt and qa (see Figure 17) from the Zimm value given by equation (45) to the Rouse value given by equation (43). It has been conjectured in the literature that the Rouse limit may be followed as polymer concentration is close to 1.

5.2.4.3. Characteristic Frequency $\Omega(q)$. *Hydrodynamic Interaction Strength B.* In cases where $S(q, t)$ can be calculated, $\Omega(q)$ can easily be

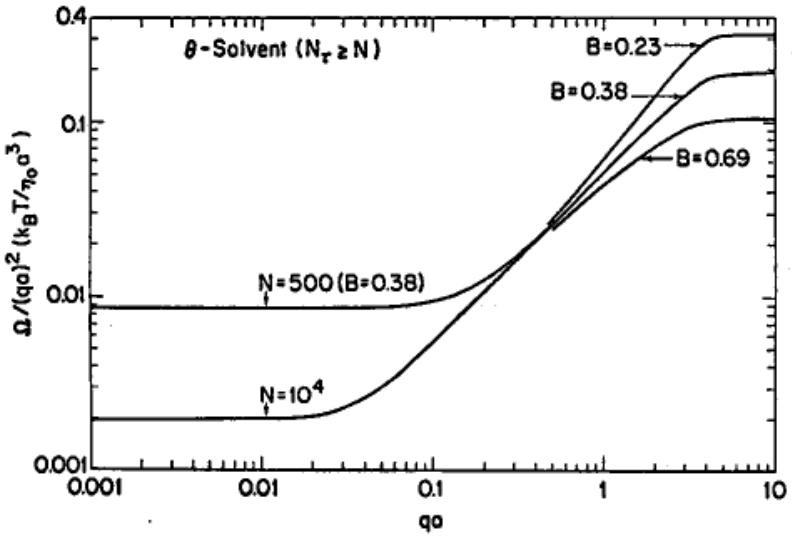

Figure 18. The variation of the initial slope $\Omega(q)$ with (qa) under Θ conditions for various values of the draining parameter B and two values of N. Note that the curves for different B's and a fixed N coincide at small values of qa.

obtained through differentiation as shown in the previous section. When $S(q, t)$ cannot be calculated, progress may still be possible by using the procedure developed by Akcasu and Gurol[34] in 1976 to calculate the characteristic frequency $\Omega(q)$. For example: the effect of preaveraging Oseen tensor can be compared for both Gaussian (or Θ) chain and excluded volume chain at different hydrodynamic interaction strength.

In Figure 18, the variation of $\Omega(q)$ with qa for a Θ chain of two different chain lengths, N, and various values of B are displayed. Notice that the curves for different B's coincide for a given N at small values of qa. The curves are plotted following equation (17) of Reference 20, are calculated with a preaveraged Oseen tensor, but the effect of preaveraging the Oseen tensor can also be studied through the Akcasu–Gurol formalism.

Preaveraging. With the preaveraged Oseen tensor, $\Omega(q)$ can be expressed in the small qa region as

$$\frac{\Omega(q)}{q^2 D_\nu} = \frac{(1-\nu)(2-\nu)}{2} \kappa_\nu \frac{\gamma((1-\nu)/2\nu, \kappa_\nu^2) - \kappa_\nu^{-1/\nu}\gamma((2-\nu)/2\nu, \kappa_\nu^2)}{\gamma(1/2\nu, \kappa_\nu^2) - \kappa_\nu^{-1/\nu}\gamma(1/\nu, \kappa_\nu^2)} \tag{47}$$

where

$$\kappa_\nu^2 \equiv (qR_g)^2(1+\nu)(1+2\nu)/3$$

$$R_g \equiv lN^\nu[2(1+\nu)(1+2\nu)]^{-1/2}$$

$$D_\nu = \frac{kT[3\pi(1+\nu)(1+2\nu)]^{-1/2}}{\eta R_g \pi(1-\nu)(2-\nu)}$$

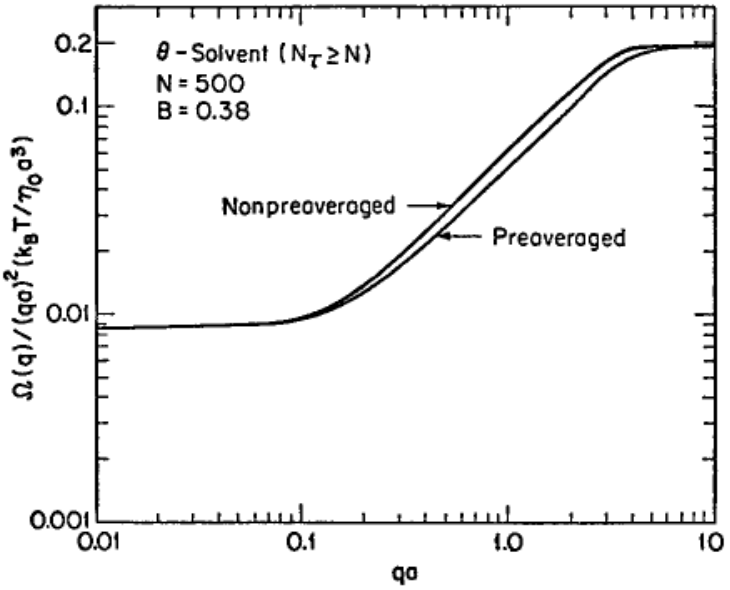

Figure 19. Variation of $\Omega(q)/q^2(kT/\eta)$ with (qa) under Θ conditions with a preaveraged and nonpreaveraged Oseen tensor. Note that the maximum difference (15%) is reached at $qa \approx 1$.

and where

$$\gamma(\mu, x) \equiv \int_0^x dt\ t^{\mu-1} \exp(-t)$$

is the incomplete gamma function. This expression yields $\Omega(q)$ in the Θ-condition with $\nu = 1/2$, and in a good solvent with $\nu = 3/5$.

The expression for $\Omega(q)$ has also been obtained without the approximation of preaveraging the Oseen tensor. Again, in the small qa region, it can be reduced as

$$\frac{\Omega(q)}{q^2 D_\nu} = \frac{3(1-\nu)(2-\nu)}{16\nu}\,\kappa_\nu^{(-1-1/\nu)}\left[\int_0^1 du\,(1-u)e^{-u^{2\nu}\kappa_\nu^2}\right]^{-1} \times \int_0^{\kappa_\nu^2} du\left(1-\frac{u^{1/2\nu}}{\kappa_\nu^{1/\nu}}\right)u^{1/2\nu-2} \times \left[-u^{-1/2} + (2+u^{-1})e^{-u}\int_0^{u^{1/2}} dt\ e^{t^2}\right] \tag{48}$$

where D_ν, κ_ν, and R_g have the same meaning as in equation (47). This result is valid for both theta and good solvents with $\nu = 1/2$ and $\nu = 3/5$, respectively.

In Figure 19, the effect of preaveraging the Oseen tensor is demonstrated for a Θ chain. The important feature is in the intermediate region

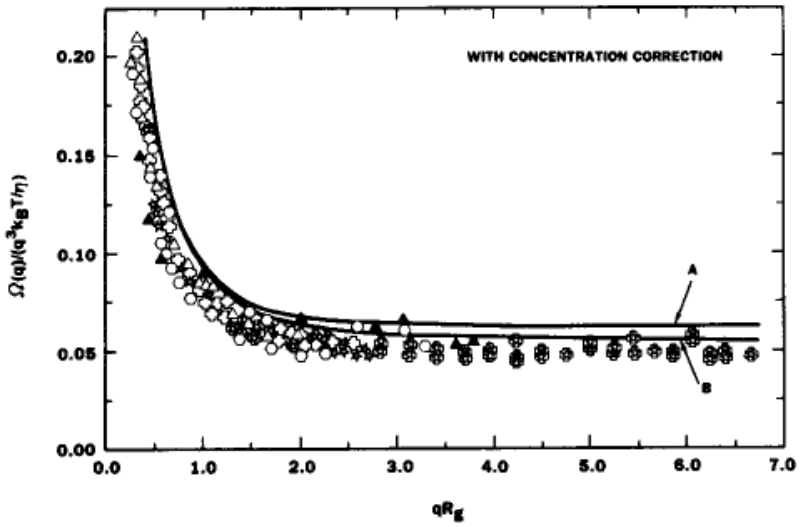

Figure 20. Variation of the reduced first cumulant Ω as a function of qR_g at the Θ condition with concentration correction.

($qa \ll 1$ and $gR_g \gg 1$). In both cases—with and without preaveraging—$\Omega(q)$ approaches q^3 dependence but with different magnitude. Actually, the same effect also appears in the excluded volume chain case.

In this intermediate q region, this effect can be summarized as follows:

For the Θ chain:

$$\Omega(q) = 0.053 \frac{kT}{\eta} q^3 \qquad \text{with preaveraged Oseen tensor}$$

$$= 0.0625 \frac{kT}{\eta} q^3 \qquad \text{without preaveraged Oseen tensor}$$

For the excluded volume chain:

$$\Omega(q) = 0.071 \frac{kT}{\eta} q^3 \qquad \text{with preaveraged Oseen tensor}$$

$$= 0.079 \frac{kT}{\eta} q^3 \qquad \text{without preaveraged Oseen tensor}$$

In Figures 20 and 21,[49] $\Omega(q)/[(kT/\eta)q^3]$ is plotted vs. qR_g for various molecular weights of polystyrene in Θ (CH, 35°C) and good (TOL and THF) solvents, respectively. Also the calculated curves according to equations (47) and (48) were included. It was concluded[49] that the dynamic light scattering experiments in the diffusion, transition, as well as in the intermediate q regions can be interpretated on the basis of the characteristic

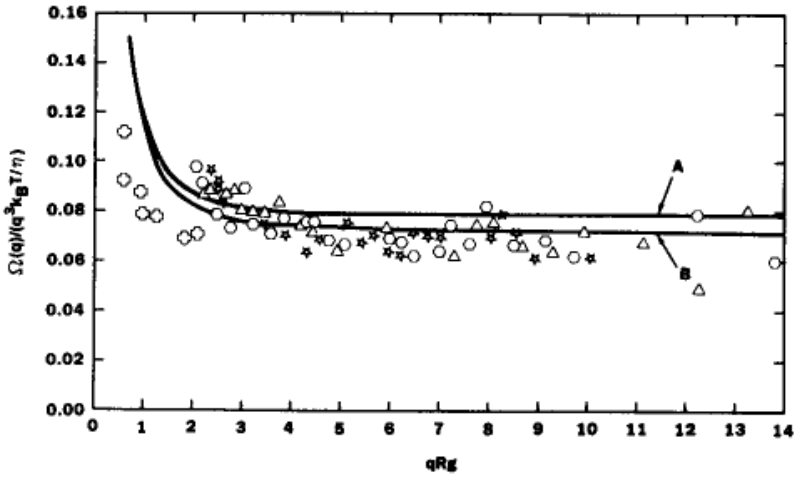

Figure 21. Variation of the reduced first cumulant Ω as a function of qR_g in good solvents. Curves A and B are the same as in Figure 20, except $\nu = 0.6$.

frequency $\Omega(q)$ as far as trends are concerned. In both Θ and excluded volume chain cases, experimental data agree better with the preaveraged Oseen tensor calculation. It is suggested that the Oseen tensor approximation needs improvement, but the preaveraged Oseen tensor calculation may be interpretated as a better model. This result, however, cannot eliminate the possibility that the equilibrium distribution function itself needs improvement, especially at short distances.

Effect of Temperature (Excluded Volume). In the previous section, we discussed two extreme cases of excluded volume effect: the Θ-chain case, which has no excluded volume at all, and the excluded-volume chain case, which has excluded volume effect everywhere along the chain. In this section, we use the blob model to demonstrate $\Omega(q)$ as a function of temperature, although we should keep in mind that $\Omega(q)$ can be calculated for a better model through the Akcasu–Gurol formalism when it is available.

In the blob model, chain statistics of mean-square distance are expressed as[8, 51, 25]

$$\langle R_{nm}^2 \rangle = |n - m| a^2 \qquad \text{if } |n - m| < N\tau \tag{49a}$$

and

$$\langle R_{nm}^2 \rangle = \left(\frac{|n - m|}{N_\tau} \right)^{2\nu} \xi_\tau^2 \qquad \text{if } |n - m| > N_\tau \tag{49b}$$

where N_τ is defined in equation (25b)

$$N_\tau \sim \tau^{-2} \tag{49c}$$

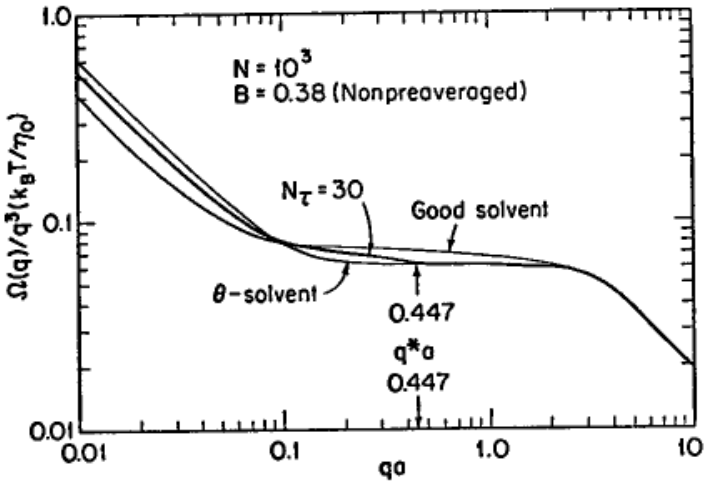

Figure 22. Variation of $\Omega(q)/q^3(kT/\eta)$ with (qa) using a nonpreaveraged Oseen tensor, in good solvent, in Θ solvent, and for an intermediate temperature corresponding to $N_\tau = 30$. This figure also illustrates the tendency to a crossover from good to Θ conditions when q is increased from $q < q^*$ to $q > q^*$.

and

$$\xi_\tau^2 = N_\tau a^2 \tag{49d}$$

The characteristic frequency $\Omega(q)$ has been calculated with[19] and without[44] preaveraging the Oseen tensor as a function of temperature $\tau \equiv (T - \Theta)/T$. In Figure 22, the effect of temperature crossover according to the blob model is illustrated. The plateau corresponding to $\Omega(q) \sim q^3$ behavior is replaced by a smooth transition from 0.0790 to 0.0625. The transition occurs at around q^*, which is defined as $q^* \equiv \sqrt{6}/\xi_\tau$.

A transition to theta behavior at high q, similar to Figure 22, has been reported by Richter *et al.*[82] using quasielastic neutron scattering. The observed crossover, however, occurs very near the temperature where PS shows a change in flexibility,[83] so it is possible that the transition represents a change in the effective segment length na rather than the crossover predicted by the blob model. For the static structure factor, no transition to theta behavior is observed[18] at high q, so it would be surprising if the dynamics reflected such a crossover. The blob model represents a severe approximation and it seems unlikely that crossovers as abrupt as Figure 22 will ever be observed.[17, 18]

5.3. VIRIAL REGIME

In this section we will discuss various predictions of the concentration dependence of diffusion constant, D, in the dilute region as a function of

temperature and molecular weights. Some experimental results are included for comparison.

The concentration dependence of D can be examined through the Gibbs–Duhem expression[5] as

$$D = \frac{kT}{\zeta_{ch}}\left(1 - \frac{N_A V_1}{M} c\right)(1 + 2A_2 Mc + \cdots) \tag{50}$$

where T is the temperature of the solution and ζ_{ch} is the frictional coefficient of the polymer molecule in solution. A_2 is the second virial coefficient of the osmotic pressure, V_1 is the partial specific volume of polymer with molecular weight M, and N_A is Avogadro's number. In this expression the concentration dependence of D is separated into two parts: The first contribution is from the chemical potential, which involves the virial coefficients. The second contribution is due to the hydrodynamic interaction, which is included in the frictional coefficient ζ_{ch}. One can immediately draw several conclusions: (i) The concentration dependence of D can be nonzero at Θ temperature, because ζ_{ch} may still be concentration dependent even at $T = \Theta$. (ii) If we write $D(c) = D(0) + Sc$, the sign and magnitude of the initial slope S of D as a function of concentration at a given temperature and molecular weight will depend on the relative magnitudes of A_2 and the concentration coefficient of ζ_{ch}.

In the theoretical calculations, the concentration dependence of D is normally expressed as

$$D(c) = D(0)(1 + k_D c_v) \tag{51}$$

with concentration coefficient k_D and concentration c_v which is the volume fraction occupied by polymer chains and defined as

$$c_v \equiv cN_A v_h / M \tag{52}$$

when v_h is the hydrodynamic volume of the polymer molecule.

In the theoretical calculation of k_D, it is the calculation of ζ_{ch}[52–57] which depends on the model and approximations used. In Figure 23, several theoretical calculations are included. Curve 5 represents the calculation of Yamakawa[5, 52] by using the bead-and-spring model with the drift velocity correction. Curve 6 is calculated by Pyun and Fixman[54] using the interpenetrable sphere model. Curve 7 is the calculation of Altenberger and Deutch[55] for hard spheres. Akcasu and Benmouna[56] and Akcasu[57] have also calculated k_D through the intermediate scattering function $S(q, t)$,

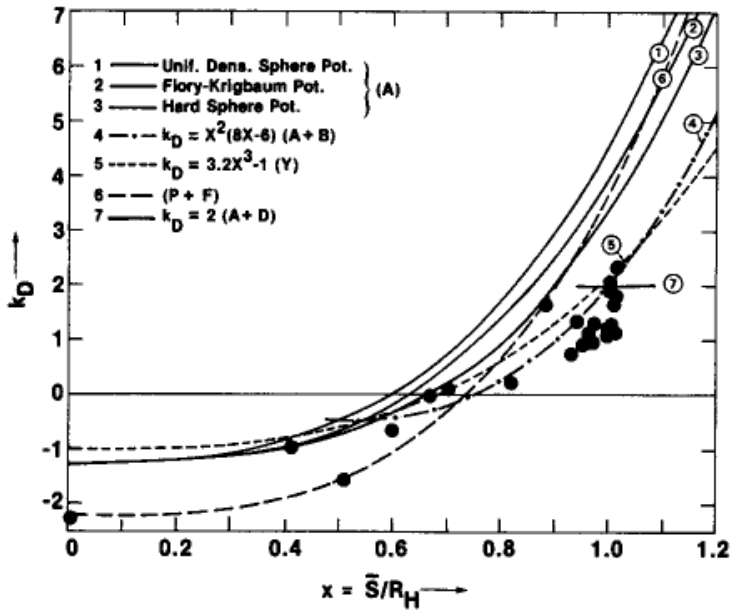

Figure 23. Second virial coefficient of the diffusion constant as a function of the ratio of the hard sphere radius to the hydrodynamic radius.

rather than using the Gibbs–Duhem formulation. In their calculation, various models and potentials (curves 1–4) were used.

Included in Figure 23 are also some experimental results for polystyrene with various molecular weights, temperature, and solvents.[23, 27, 58] All models and experimental results show similar trends as regards the temperature dependence of k_D except for the hard sphere model, which does not apply at lower temperature. In all cases, k_D vanishes at a temperature corresponding to $\bar{S}/R_h \cong 0.72$ with $\bar{S}$ defined as $(3M^2A_2/16\pi N_A)^{1/3}$. This value of $\bar{S}/R_h$ marks the transition from theta to good solvent behavior. In the good solvent region $k_D > 0$ and the diffusion coefficient increases with concentration. In this region, Yamakawa's result (curve 5) and that of Akcasu *et al.*[56] (curve 4) are in good agreement with experimental results. The assumption of replacing the distance between two monomers belonging to two different molecules by their center-of-mass separation[56] is justified probably because the molecular interpenetration is not serious. This assumption could be the cause of $k_D = 0$ at Θ condition in the calculation of Akcasu *et al.* where the molecular interpenetration could be significant.

In the poor solvent region, $k_D < 0$ and the theoretical predictions are very sensitive to the models used to describe the translational diffusion of a pair of interacting molecules. Calculations of Pyun and Fixman,[54] Yamakawa,[52] and Akcasu[57] all give correct negative k_D. But it seems that more refined models and more precise measurements are still needed in this region.

5.4. SEMIDILUTE SOLUTIONS

5.4.1. Introduction

As the concentration of a polymer solution is increased, eventually the virial expansion [equation (51)] is inadequate. The virial method would certainly be inadequate when the chains begin to overlap and entangle because new dynamical processes involving interchain interactions and disentanglement come into the problem. The number concentration at the overlap is approximately

$$\rho^* \simeq \frac{3N}{4\pi R_g^3} \tag{53}$$

and virial expansions certainly fail for $\rho > \rho^*$. For typical polymers ($N \sim 1000$), chain overlap occurs at concentrations of about 1% by volume. In a sense then the solution is still dilute since a particular monomer is still surrounded overwhelmingly by solvent molecules and seldom is in contact with monomers. The regime $\rho^* \ll \rho \ll a^{-3}$ is called the semidilute regime. The system is dilute in terms of overall monomer density but the system still displays strong dynamical effects due to the interchain contacts.

The transition from dilute to semidilute is illustrated in Figures 24 and 25, which show the mean relaxation rate Ω/q^2 for polystyrene of various

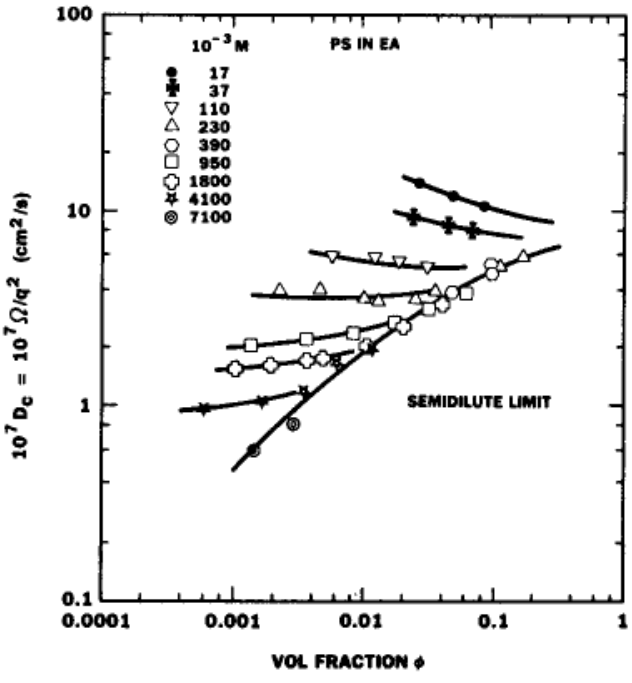

Figure 24. Concentration dependence of the relaxation rate for PS in EA[22] in the dilute and semidilute region at 25°C. ρ^* is defined as the concentration where the molecular-weight-dependent dilute curves intersect the semidilute limit. EA is a near theta solvent. At low concentration the ordinate is the self-diffusion constant and at high concentration it is the collective diffusion constant.

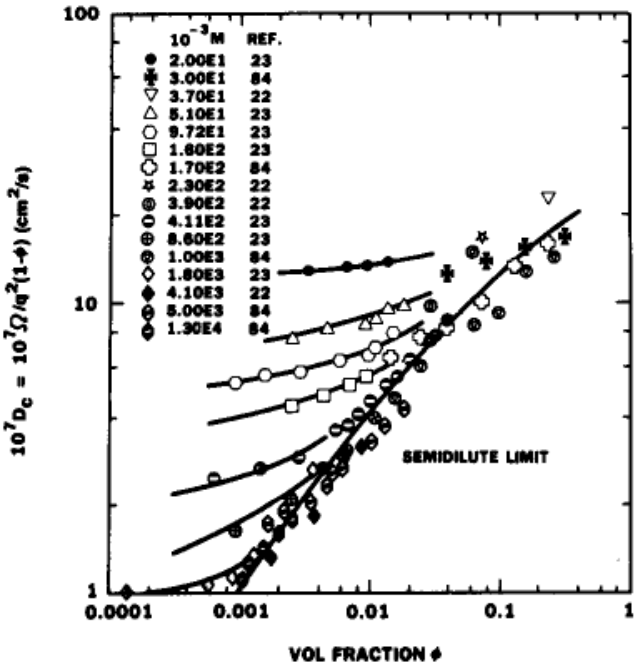

Figure 25. Concentration dependence of the relaxation rate for PS in THF. All the data have been reduced to 25°C. Substantial scatter between different groups is found, particularly at high concentration.

molecular weights in ethyl acetate (EA) and tetrahydrofuran (THF). Several observations can be made concerning these data, the most important of which is that the Ω becomes independent of molecular weight at concentrations near ρ^*. The regime where Ω is independent of molecular weight is called semidilute and the molecular-weight independence results from the fact that concentration fluctuations relax without overall chain motion. It should also be noted that for a given molecular weight the semidilute regime occurs at higher concentrations in marginal solvents (EA) than good solvents (THF). This difference is a consequence of the greater degree of swelling in good solvents.

In contrast to dilute systems, the dynamics of semidilute solutions are not firmly established either theoretically or experimentally. On the theoretical side, the results of the self-consistent field calculation of Freed and Edwards[59] contrasts with the scaling approach of de Gennes.[12] Contradictory experiments also exist with inconsistent conclusions reported by different groups working on the same system. In some sense then, it is premature to review semidilute systems at this time. Nevertheless, this report is more optimistic and an attempt is made to resolve the body of conflicting information through a careful identification of the conditions under which theoretical assumptions are satisfied. The general approach is that of Reference 22, although the details of the model are somewhat refined.

5.4.1.1. Hydrodynamic Screening. The concept of hydrodynamic screening is central to the understanding of semidilute polymer solutions.

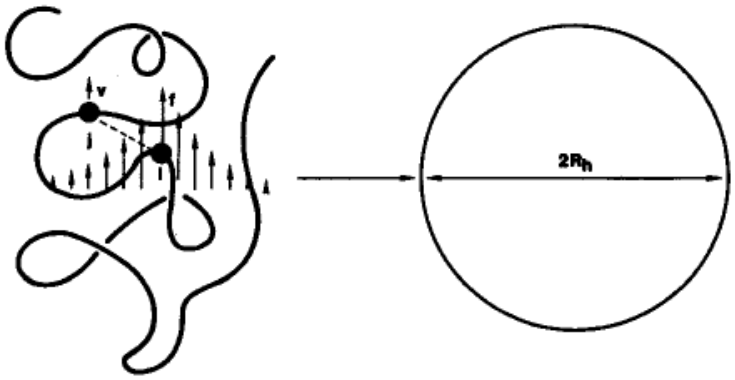

Figure 26. Schematic picture of the hydrodynamics of a single chain. A force f is exerted on the solvent by monomer i. This force leads to a solvent flow field decaying as $1/r$. This flow field leads to a solvent velocity at monomer j which couples the motion of the two monomers. If the flow fields of all monomers are summed self-consistently, then the chain friction constant is the same as that of a sphere of radius $R_h = \langle 1/r \rangle^{-1}$, where r is the intersegment distance in the chain.

Screening can be understood by first recalling the situation for a single chain in dilute solution. Here, the Kirkwood–Riseman calculation[10] shows that the solvent flow caused by the motion of any monomer leads to a solvent-mediated coupling with other monomers in the chain. In fact, in the regime of $qR \ll 1$, the motion of the chain is equivalent to that of a hard sphere of the same hydrodynamic radius. This situation is represented schematically in Figure 26 where the flow field around a single moving monomer is shown as well as the equivalent hard sphere.

In semidilute solution, the single-chain picture remains correct for short distances. That is, short sequences are coupled hydrodynamically and tend to move in a correlated manner. The situation for widely separated monomers on the same chain, however, is quite different because a distant monomer also feels the flow field caused by monomers on other chains. The flow fields from the neighboring chains are not correlated with that arising from monomers on the same chain so that the motion of widely separated monomers on the same chain becomes uncorrelated. This situation is shown schematically in Figure 27, which shows the equivalent hard sphere picture of a semidilute solution. Conceptually the system is replaced by a space-filling (or in some cases overlapping) group of spheres (concentration blobs of radius ξ_ρ) whose motion is uncorrelated. The radius of the spheres, ξ_ρ, is roughly the distance between interchain contacts and is proportional to the range of the static pair correlation function. Experiments sensitive to distances small compared to ξ_ρ ($q\xi_\rho \gg 1$) should yield results similar to a single chain, whereas in the opposite limit ($q\xi_\rho \ll 1$) dynamics characteristic of the diffusion of sphere of radius ξ_ρ are observed.

The characteristic length ξ_ρ is called a screening length. In fact, the

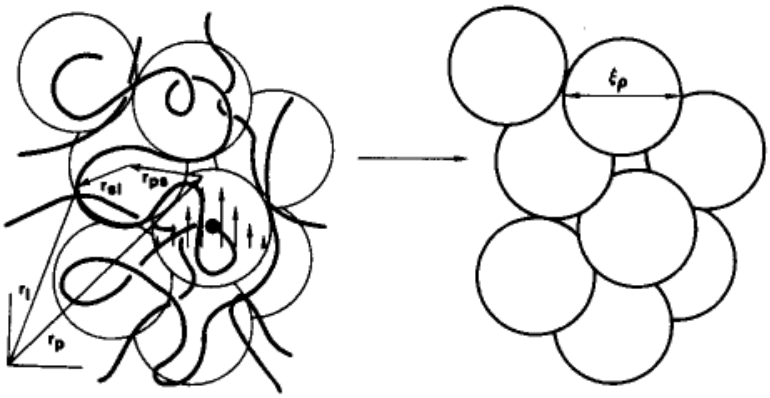

Figure 27. Schematic picture of screening in semidilute solution. In contrast to Figure 26, the flow-induced coupling is shorter ranged since distant monomers feel the random fields induced by the uncorrelated motion of monomers on other chains. The blob picture on the right shows the size of the effective Rouse blob in semidilute solution. Hydrodynamic coupling exists within the blob, but the motion of different blobs is uncorrelated even though they may share a common chain.

radial dependence of flow field (screened Oseen tensor) in semidilute solution has the classic Debye–Huckle form[59]

$$G(r) \sim \frac{1}{r} e^{-r/\xi_\rho} \tag{54}$$

and thus the identification of ξ_ρ as a screening length. Equation (54) contrasts with the flow field in dilute solution which is described by the Oseen tensor whose radial dependence decays as $1/r$. A reasonable body of evidence[22] shows that the screening length ξ_ρ is proportional to the range of the pair correlation function. This proportionality is reasonable since in the Kirkwood–Riseman picture, interchain contacts determine both the range of the pair correlation function as well as the range of hydrodynamic interaction.[4]

An alternative but equivalent description[12] of semidilute polymers can be obtained from a balance of elastic and frictional forces. The elastic force arises from the osmotic rigidity of the transient network formed by interchain contacts and the frictional resistance is that of a blob described above. The term "pseudogel" is often used to describe semidilute solutions when $q\xi_\rho \ll 1 \ll qR_g$. This term reflects the similarities between the transient network in semidilute solution and the permanent network in crosslinked swollen gels.

5.4.1.2. Reptation. In addition to screening and concentration blobs, one further concept, reptation, is necessary to appreciate semidilute-polymer dynamics. Reptation is the snakelike motion by which a chain

completely renews its configuration.[4, 66] In congested systems, an individual chain is severely restricted by neighboring chains and effectively moves in a "tube" created by surrounding chains.[4] The reptation time T_R is the time required for a chain to completely escape a given tube and thereby renew its configuration. When the relaxation time of concentration blobs (described above) becomes comparable to T_R, then analogy to gels breaks down and a new dynamical process involving overall chain motion is important. Later we show that the reptation becomes the dominant process for $g^2 R_g^2 \ll \rho^*/\rho$.

5.4.2. Dynamical Regimes

The aspects of polymer dynamics which are probed by PCS are contained in the intermediate scattering function $S(q, t)$ in equation (5). A complete theory for $S(q, t, \rho)$ is obviously a formidable many-body problem so it is not surprising that simplified models are necessary. Fortunately, armed with the concepts of hydrodynamic screening, concentration blobs, pseudogels, and reptation, it is possible to predict the general properties of $S(q, t, \rho)$. A developing body of experimental evidence confirms many of these predictions.

Following Figure 27, $S(q, t)$ can be broken down into contributions due to chains p, concentration blobs or "strands" s within chains, and monomers i, j within strands. If $\mathbf{r}_i = \mathbf{r}_p + \mathbf{r}_{ps} + \mathbf{r}_{si}$ is the position of monomer i, then

$$\begin{aligned} S(q, t) = \frac{1}{V} \Bigg\langle & \sum_p \exp\{i\mathbf{q} \cdot [\mathbf{r}_p(0) - \mathbf{r}_p(t)]\} \sum_s \exp\{i\mathbf{q} \cdot [\mathbf{r}_{ps}(0) - \mathbf{r}_{ps}(t)]\} \\ & \times \sum_{ij} \exp\{i\mathbf{q} \cdot [\mathbf{r}_{si}(0) - \mathbf{r}_{sj}(t)]\} \\ & + \sum_p \exp\{i\mathbf{q} \cdot [\mathbf{r}_p(0) - \mathbf{r}_p(t)]\} \sum_{s \neq s'} \exp\{i\mathbf{q} \cdot [\mathbf{r}_{ps}(0) - \mathbf{r}_{ps'}(t)]\} \\ & \times \sum_{ij} \exp\{i\mathbf{q} \cdot [\mathbf{r}_{si}(0) - \mathbf{r}_{s'j}(t)]\} \Bigg\rangle \end{aligned} \tag{55}$$

Equation (55) presumes that the center-of-mass $\mathbf{r}_p$ of different chains is uncorrelated. This assumption is true in dilute solution and is also true within the reptation model of semidilute solutions. In order to simplify $S(q, t)$, it is convenient to specialize to three dynamical regimes and to

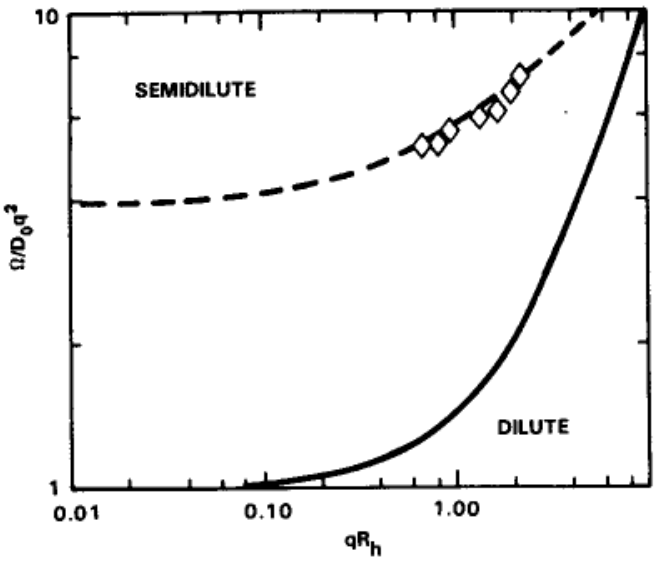

Figure 28. Comparison of the q dependence of the relaxation rate in dilute and semidilute solutions. The solid line is a best fit to the data in Figure 4, and the points are for a semidilute solution of PS in THF ($M = 4.1 \times 10^6$, $c = 0.01$ g/ml). The dotted line is to guide the eye. The blob model implies that the dotted line would intersect the solid line near $q\xi_\rho = 1$ and that the asymptote to the ordinate occurs at $\Omega/D_0q^2 = R_h/\xi_\rho$.

examine the concentration dependence of the relaxation processes within each dynamical regime separately.

5.4.2.1. The Single-Chain Limit: $q\xi_\rho \gg 1$. In the regime $q\xi_\rho \gg 1$, fast relaxation processes characteristic of monomer motion within strands dominate. In this limit $\mathbf{r}_p(0) = \mathbf{r}_p(t)$ and $\mathbf{r}_{ps}(0) = \mathbf{r}_{ps}(t)$ so equation (55) becomes

$$S(q, t) = \rho g_\rho \langle \exp\{i\mathbf{q} \cdot [\mathbf{r}_{si}(0) - \mathbf{r}_{sj}(t)]\} \rangle \tag{56}$$

where the correlation function in equation (56) has been examined in Section 5.2.2.3 by scaling and in Section 5.2.4 by linear response theory. Basically single-chain dynamics are recovered with the mean relaxation rate Ω scaling as q^3 as in equation (22).

Figure 28 shows data in the regime $q\xi_\rho \gtrsim 1$ for PS in semidilute solution. The line in the figure is the line which fit a similar plot (Figure 4) for polystyrene in dilute solution. The data in Figure 28 are not extensive, but it suggests that the crossover to q^3 scaling occurs over a very broad range in q. It is also possible that the transition to q^3 behavior occurs at $qR_h = 1$ rather than at $q\xi_\rho = 1$ as expected from the blob model. Clearly, more experimental data are needed.

5.2.2.2. The Pseudogel Regime: $q\xi_\rho \ll 1 \ll qR_g$. When $q\xi_\rho \ll 1 \ll qR_g$, equation (55) becomes

$$S(q, t) = \frac{\rho}{g_\rho} \langle g_\rho^2 \exp\{i\mathbf{q} \cdot [\mathbf{r}_{ps}(0) - \mathbf{r}_{ps}(t)]\}\rangle \tag{57}$$

where ρ is the monomer concentration and g_ρ is the number of monomers in a blob of radius ξ_ρ. Equation (57) assumes different blobs are uncorrelated due to screening as discussed above. In this equation we are concerned with the motion of the center of mass of a concentration blob whose dynamical properties have been obtained by de Gennes through analogy to cross-linked gels.[12] Equation (57) requires a Fokker–Plank equation for the time-dependent distribution function $P(\Delta r_{ps}; t)$ for the center of mass $\mathbf{r}_{ps}$ of a piece of chain between interchain contacts. The Fourier components of this distribution function, however, should follow the same dynamical equation as the Fourier components of the displacement $\mathbf{r} = \mathbf{r}_{ps}$ as Tanaka[72] assumed for his calculation of $S(q, t)$ for cross-linked gels. The equation of motion for $P(\Delta r; t)$ is determined by a balance of osmotic and frictional forces which lead to a Fourier-transformed dynamical equation of this form[63, 65].

$$-E_0 q^2 P(q; t) = \frac{\rho}{g_\rho} \zeta_\rho (1 - \phi)^{-1} \dot{P}(q; t) \tag{58}$$

where P is the distribution function hidden in equation (57), $E_0 = c\, \partial\pi/\partial c$ is the osmotic rigidity, $\zeta_\rho \simeq 6\pi\eta\xi_\rho$ is the blob friction constant, and ρ/g_ρ is the density of blobs. Solving for P in equation (58) and using (57), we obtain

$$S(q, t) = \frac{\rho}{g_\rho} \langle g_\rho^2 \exp[-D_c(1 - \phi)q^2 t]\rangle_{\xi_\rho} \simeq \rho g_\rho e^{-\Omega t} \tag{59}$$

$$\frac{\Omega}{(1 - \phi)q^2} = D_c \cong \frac{E_0 g_\rho}{\rho 6\pi\eta\xi_\rho} \tag{60}$$

Here D_c is the cooperative diffusion constant. The average over ξ_ρ in equation (59) arises because there is a distribution in blob radii ξ_ρ which is determined by the monomer pair correlation function. Experiments in cross-linked gels show that measured correlation functions are nearly exponential, so little generality is lost if the final average is ignored and ξ_ρ is identified with the range of the pair correlation function.[22] The various parameters in equation (60) depend on solvent quality (i.e., temperature), so to predict the concentration dependence of the decay rate g_ρ, ξ_ρ, and E_0 must be determined. With the exception of theta systems all these parameters depend on the probability of binary contacts.

Good Solvents. In good solvents the osmotic rigidity E_0 follows from scaling analysis.[73] In the semidilute regime the osmotic pressure is presumed to follow the power law

$$\pi \sim \frac{\rho}{N}\left(\frac{\rho}{\rho^*}\right)^x; \qquad \rho \gg \rho^* \tag{61}$$

where $\rho^* \sim N^{-4/5}$ [see equation (54)] and the exponent is fixed by the requirement that π be independent of N for $\rho > \rho^*$. This requirement leads to $x = 5/4$ so

$$\pi \sim \rho^{9/4} \tag{62}$$

Equation (62) is now well confirmed for polymers in good solvents.[70]

The osmotic rigidity $E_0 \sim \rho\, \partial\pi/\partial\rho$ immediately follows from (62):

$$E_0 \sim \rho^{9/4} \tag{63}$$

Since π is proportional to the number of binary contacts between chains, the number of monomers between binary contacts g_2 also follows. That is, since ρ/N is the number of chains per unit volume, $\rho^{9/4}(N/\rho) = N\rho^{5/4}$ is the number of binary contacts per chain. Therefore,

$$\frac{N}{g_2} \sim N\rho^{5/4} \tag{64}$$

or

$$g_2 \sim \rho^{-5/4} \tag{65}$$

In good solvents $g_\rho = g_2$ since concentration blobs are identified with strands between binary contacts.

The distance $\xi_\rho \sim \xi_2$ between contacts follows

$$\xi_\rho \sim g_2^{3/5} a \sim \rho^{-3/4} \tag{66a}$$

$$\simeq a\phi^{-3/4} n^{-1/4}(1 - 2\chi)^{-1/4} \tag{66b}$$

using equation (2). ϕ is the monomer volume fraction. Equation (66b) does not follow directly from the simple arguments presented here.[22, 74]

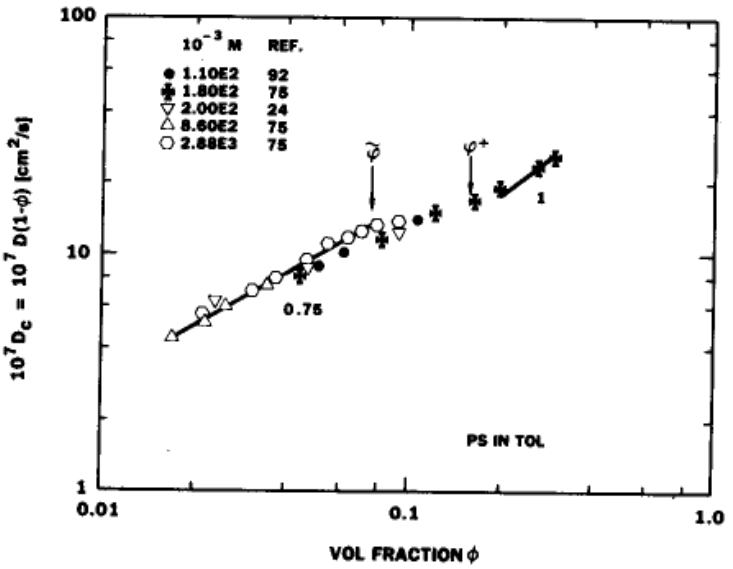

Figure 29. Concentration dependence of the collective diffusion constant D_c for polystyrene in semidilute solution in toluene. Toluene is a good solvent and scaling is observed below $\phi = 0.08$. This data may show a small marginal regime between $\tilde{\phi}$ and $\phi^\dagger$. All the data have been corrected to 25°C. Most of these data were measured by gradient diffusion. The data for the 1.8×10^6 sample due to Rehage and Ernst and are recorded in Reference 75.

In semidilute good solvents, density dependence of the relaxation rate Ω follows from equations (60), (63), (65), and (66):

$$D_c = \frac{\Omega}{q^2(1-\phi)} \sim \rho^{3/4} \sim \phi^{3/4} \tag{67}$$

For reasons which should become clear later, the scaling law equation (67) is seldom observed experimentally. Although scaling behavior has been claimed for many systems, it appears that only the PS/TOL and PDMS/TOL systems show unequivocal scaling exponents. From Table 1, these two systems represent a very good solvent (N_τ small for PS in TOL) and a very flexible molecule ($n \cong 1$ for PDMS). In addition to these two systems, the work of Yu *et al.*[68] shows a clear scaling regime for PS in THF at 30°C. These data, however, seem inconsistent with other data on PS in THF at 25°C, so they will be analyzed later.

Figure 29 shows data on semidilute PS in TOL obtained both by PCS and by gradient diffusion. This latter method is expected to yield the cooperative diffusion constant D_c when the gradient is small.[50] The data in Figure 29 are consistent with equation (67) for $\phi < 0.07$. Above $\phi = 0.07$ there appears to be two transitions which are discussed below.

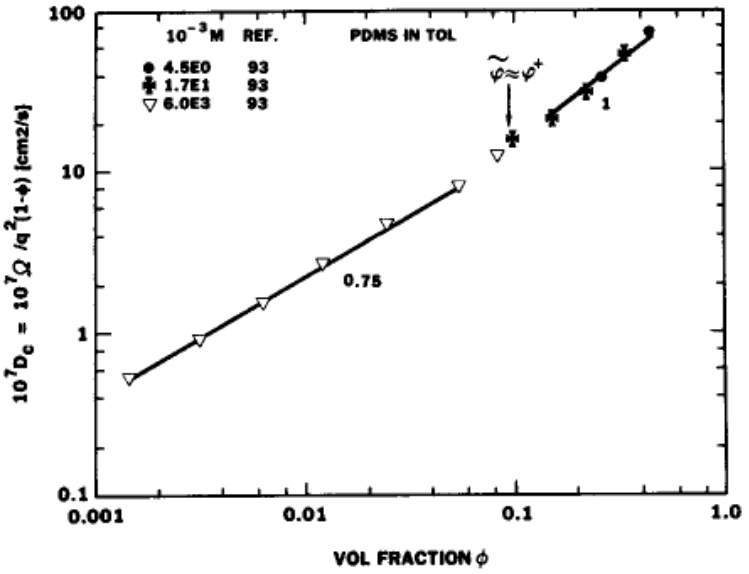

Figure 30. Concentration dependence of the collective diffusion constant for polydimethylsiloxane (PDMS) in toluene. PDMS is a very flexible chain, so no marginal regime is observed. $T = 20°C$.

PDMS is a very flexible molecule with $n = C_\infty/6 \simeq 1$. This system also shows a large region in semidilute solution where the scaling law is obeyed. The data of Munch *et al.*[92] for this system are shown in Figure 30 with a line of slope = 0.75 drawn through the data below $\phi = 0.1$. Above $\phi = 0.1$ a transition to a larger slope is observed. Below we show that such a transition is expected for a very flexible chain.

The breakdown of scaling at high concentration is due to the fact that the chains are ideal at small length scales in contrast to the assumption of equation (67), which depends on the fact that the chains are swollen: i.e., $\xi_\rho \sim g_\rho^{3/5}$. We know from Section 5.2.3 that swelling is found only for distances greater than ξ_τ, the temperature-dependent length which characterizes the statistics of the single chain. The volume fraction $\tilde{\phi}$ where equation (67) breaks down is found from equating ξ_ρ in equation (66) with ξ_τ in equation (25) or

$$\tilde{\phi} \cong \frac{3(1 - 2\chi)}{4\pi n^3} \tag{68}$$

$\tilde{\phi}$ is tabulated in Table 4 for several systems. Note that the predicted cutoff for scaling behavior is generally below $\phi = 0.05$.

Marginal Solvents. Above $\tilde{\phi}$ the chains are nearly ideal on all length scales and binary interactions are weak. In such a system, binary contacts occur at random with a probability proportional to $\phi^2 \sim \rho^2$. Following the

Table 3. Exponents for the Density Dependence of Various Quantities[a]

Quantity	Good	Marginal	Theta	Quantity	Good	Marginal	Theta
g_ρ	$-5/4$	-1	-2	D_c	3/4	1/2	1
ξ_ρ	$-3/4$	$-1/2$	-1	T_R/N^3	3/2	5/2	3
g_2	$-5/4$	-1	-1	E_0	9/4	2	3
ξ_2	$-3/4$	$-1/2$	$-1/2$	E_{gel}	9/4	2	2
g_3	—	-2	-2	N^2D_s	$-7/4$	$-5/2$	-3
ξ_3	—	-1	-1	η_r/N^3	15/4	9/2	5
g_t	$-5/4$	-2	-2	s	$-1/2$	$-1/2$	-1
ξ_t	$-3/4$	-1	-1				

[a] ξ_ρ is the range of the pair correlation function and is proportional to the hydrodynamic screening length. ξ_2 and ξ_3 are the distance between binary and ternary contacts. ξ_t is the radius in the repetation model. g_ρ, g_2, g_3, g_t are the number of monomers associated with the above lengths. T_R is the tube renewal time. E^0 and E_{gel} are the osmotic and elastic moduli. D_s is the self-diffusion coefficient. η is the viscosity, and s is the sedimentation constant.

logic of equations (64)–(66) then, one finds

$$\pi \sim E_0 \sim \rho^2 \tag{69}$$

$$g_\rho \sim g_2 \sim \rho^{-1} \tag{70}$$

$$\xi_\rho \sim \xi_2 \sim g_2^{1/2} a \sim \rho^{-1/2} \tag{71}$$

$$\cong \frac{n^{3/2}a}{(va^{-3})^{1/2}}\,\phi^{-1/2} \tag{72}$$

or using equation (60)

$$D_c = \frac{\Omega}{q^2(1-\phi)} \sim \phi^{1/2} \tag{73}$$

Once again, the coefficients in equation (72) do not follow directly,[22] but this equation will be useful later.

Experimental results consistent with equation (73) are observed in a large number of systems.[22, 64, 75, 78] Figures 31 and 32, for example, show PS in EA and MEK. Both systems show over a decade in concentration where $D_c \sim \phi^{1/2}$ is predicted by equation (73). Table 1 shows that these systems are marginal in the sense that excluded volume effects are weak but not absent ($N_\tau \simeq 10^3$). These solvents are generally called marginal solvents

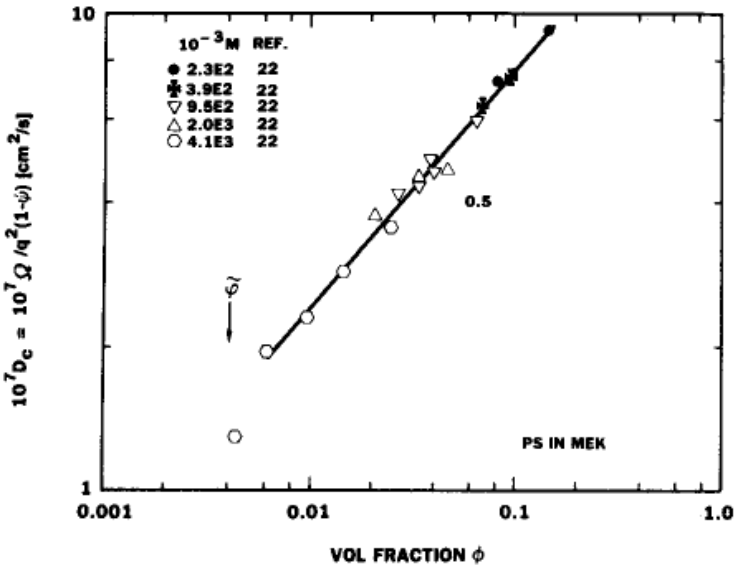

Figure 31. Concentration dependence of the collective diffusion constant for PS in MEK at 25°C.

and the regime above $\tilde{\phi}$ is called marginal semidilute. In the PS/MEK system there is a hint of a transition to steeper slope or scaling behavior below $\tilde{\phi} \cong 0.004$. In the PS/EA system, on the other hand, there appears to be a transition to steeper slope above $\phi = 0.08$. These transitions are probably manifestation of similar behavior found in PS/TOL in Figure 29. Other systems have been studied which may show marginal behavior such as PS/BZ and PS/THF. Interpretation of these systems is more complex, however, so discussion is deferred until the end of this section. PAMS dissolved in toluene[78] and PS in ethylbenzene and chlorobenzene[75] also show marginal behavior for $\phi > 0.01$. These observations are reasonably consistent with $\tilde{\phi}$ calculated from equation (68) using N_τ from Table 1.

Marginal systems described by equation (73) are usually associated with Edwards, who first obtained equation (73) in the mean-field approximation. Because of this approximation this regime is also called the mean-field regime. To confuse the situation further, British scientists often call $\phi > \tilde{\phi}$ the semiconcentrated regime. Continental scientists generally treat the marginal regime with patched-up scaling laws.[45, 95]

Theta Systems. As the concentration is increased or the binary interaction parameter, $va^{-3} = 1 - 2\chi$, is decreased and eventually three-body interactions dominate two-body effects. This situation can be expected either near the theta temperature or at high concentration. These systems, which are generically referred to as theta systems, cannot be described by

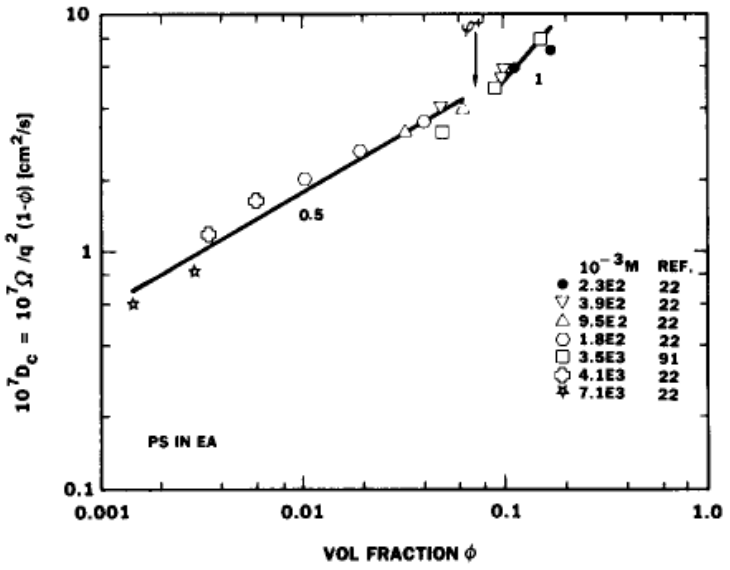

Figure 32. Concentration dependence of the collective diffusion constant for PS in ethyl acetate at 25°C.

the preceding theory where two-body interactions determine E_0, g_ρ, and ξ_ρ. In theta systems, both the osmotic pressure and osmotic rigidity E_0 are proportional to the probability of ternary contacts:

$$E_0 \sim E_3 \sim \rho^3 \tag{74}$$

Therefore, the blob friction constant in equations (58) and (60) must be calculated for a strand spanning ternary contacts that is $\xi_\rho \sim \xi_3$ and $g_\rho \sim g_3$,

$$g_\rho \sim g_3 \sim \rho^{-2} \tag{75}$$

$$\xi_\rho \sim \xi_3 \sim g_3^{1/2} a \sim \rho^{-1} \tag{76}$$

$$\simeq \frac{an^2}{(wa^{-6})^{1/2}} \phi^{-1} \tag{77}$$

where w is the three-body excluded volume ($w \simeq a^6 n_3$). Equation (77) was first obtained by Moore for the static correlation range[76] and was applied by Schaefer *et al.*[22] to dynamics. Application of equations (74)–(77) to equation (60) yields

$$D_c = \frac{\Omega}{q^2(1-\phi)} \sim \rho \sim \phi \tag{78}$$

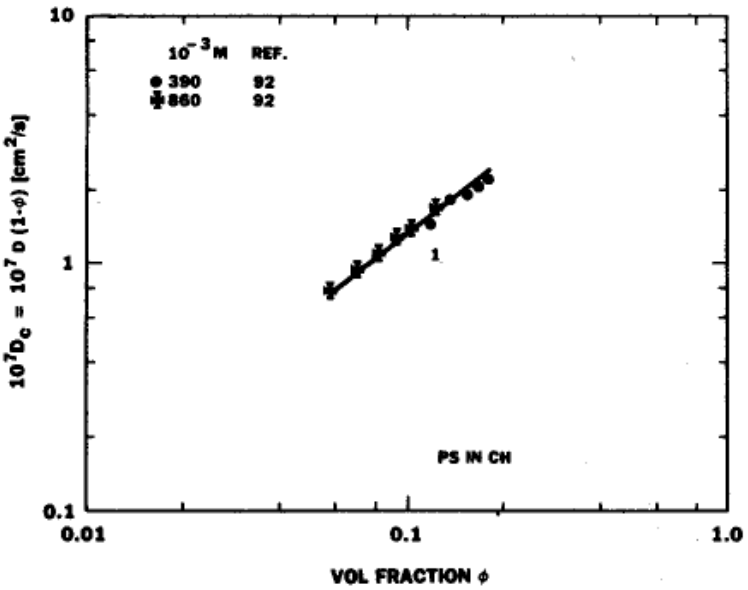

Figure 33. Concentration dependence of the collective diffusion constant of PS in cyclohexane at the theta temperature. Data were obtained by gradient diffusion.

Equation (78) is expected to apply to theta solvents for all concentrations above ρ^* and to other systems where the ρ is high enough that three-body effects dominate. This concentration, $\rho^\dagger$, can be found by equating equation (77) with equation (72) assuming $w = n^3a^6$,

$$\phi^\dagger = \rho^\dagger a^3 \simeq (1 - 2\chi) \tag{79}$$

This equation is highly approximate since the assumption $w = a^6n^3$ is unverified. For a few systems,[77] v and w are known from static properties and it appears that equation (79) is correct within a factor of 3.

Unfortunately, experimental data on cooperative diffusion in theta solvents are very limited. This scarcity is due to the fact that very high molecular weights are required to achieve chain overlap below $\phi = 0.1$. In theta solvents, however, high molecular weight chains are heavily self-entangled, making it difficult to achieve equilibrium systems. In fact, months or even years may be required to prepare such systems.[93]

Although PCS data is lacking on theta systems, both gradient diffusion[88] and sedimentation[75] results exist which are consistent with equation (78). Figure 33, for example, shows Roots and Nystrom's gradient diffusion data[88] for PS in CH at the theta temperature. Although the concentration range covered is limited, the data are consistent with a power law exponent of 1.0.

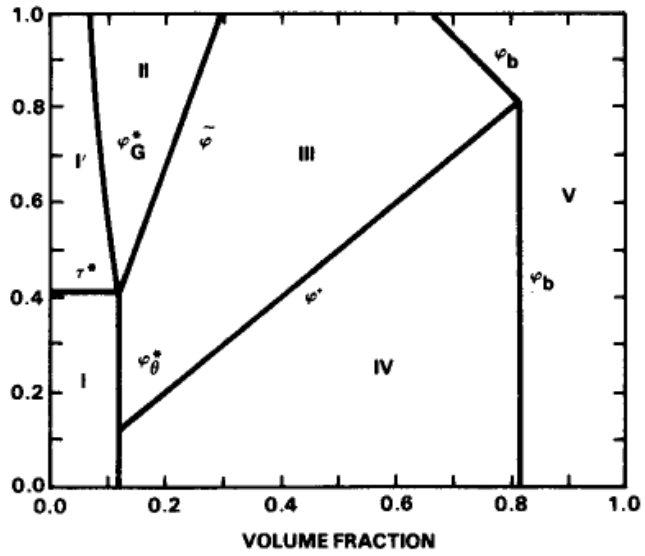

Figure 34. T–C diagram for a 20-unit chain with $n = 1.5$. The excluded volume parameter v is assumed to be linear in the temperature increment $\tau = (T - \Theta)/T$.

Thetalike behavior is also observed in good and marginal solvents at high concentration. The systems PS/TOL, PS/EA, and PDMS/TOL in Figures 29–31 all show power-law exponents near unity at high concentration. There are numerous potential experimental problems at high concentration, so these Θ-like exponents above $\phi = 0.1$ may be questionable. In fact, several workers have observed concentration independence or negative exponents at high concentration.[22, 60]

T–C Diagrams. The various pseudogel regimes described above can be collected graphically through a temperature-concentration diagram (T–C diagram) as proposed by Daoud and Jannink.[80] Such a diagram is shown in Figure 34 for a 20-unit chain with $n = 1.5$ and $(1 - 2\chi) = \tau$. The various lines in the figure represent the approximate transition regions where the nature of polymer dynamics changes. The line τ^*, for example, separates dilute theta systems (region I) from dilute swollen systems (region I'). The equation for this line follows from equation (25b) with $N_\tau = N$. Lines ϕ_Θ^* and ϕ_G^* represent the crossover to semidilute solution and follow from equation (53) for theta and good solvents.

As discussed above, the semidilute regime is subdivided into good (II), marginal (III), and theta (IV) domains with the crossovers $\tilde{\phi}$ and $\phi^\dagger$ defined by equations (68) and (79). Finally, the crossovers ϕ_b to the concentrated regime V are determined by the condition $\xi_\rho = na$ and follow directly from equations (72) and (77).

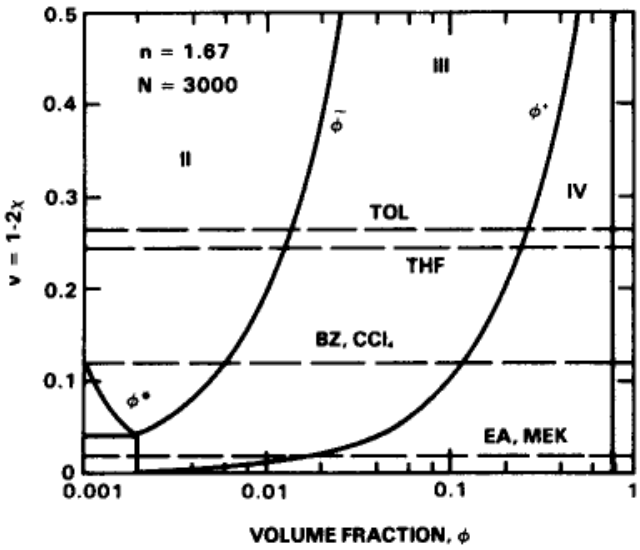

Figure 35. T–C diagram for PS. The ordinate is the coupling constant $(1 - 2\chi) = va^{-3}$ and various solvents are represented by the horizontal lines.

A more universal form of the T–C diagram can be constructed by use of the parameter $(1 - 2\chi) = va^{-3}$ instead of temperature on the ordinate. The semilog version of such a plot is shown in Figure 35 for $N = 3000$ and $n = 1.67$. This value of n is chosen for PS where $n = C_\infty/6 = 1.67$ when equation (1) is applied to the radius of gyration. The behavior of PS in various solvents can be predicted from horizontal lines at the appropriate values of $(1 - 2\chi)$ obtained from Table 1. Lines appropriate to several solvents are included. Plots like Figure 35 should accurately reflect trends with temperature, chain rigidity, and solvent quality, but caution should be exercised in quantitative predictions based on the diagrams. After all, the assumptions leading to the diagram are crude, and although power law exponents are probably accurate, the coefficients required for quantitative analysis are largely unknown.

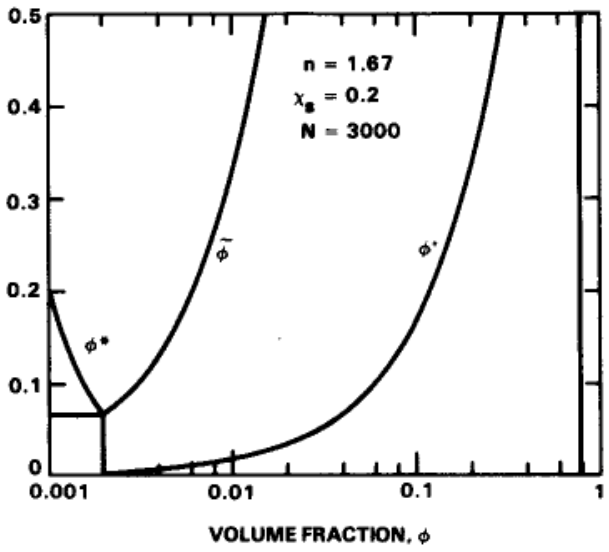

Figure 36. T–C diagram for PS in cyclohexane. This diagram assumes $\chi_s = 0.2$ and that $(1 - 2\chi)$ is linear in the temperature increment $\tau = (T - \Theta)/T$.

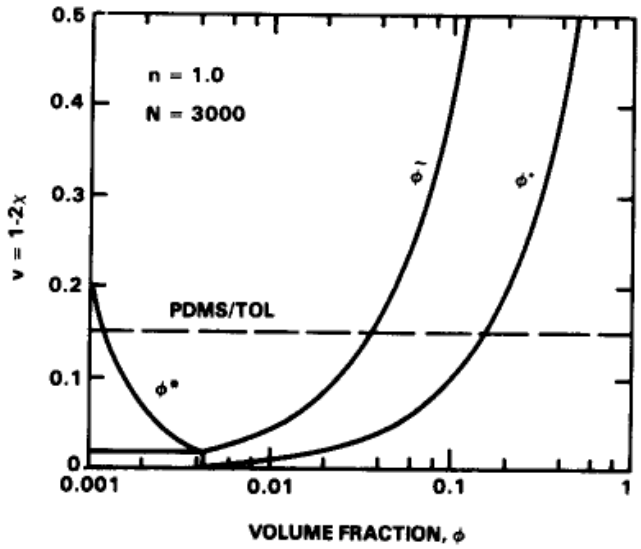

Figure 37. *T–C* diagram for a completely flexible chain. This diagram should be appropriate for PDMS. $1-2\chi$ for PDMS in toluene is shown as a horizontal line.

For systems like PS in CH where va^{-3} is a strong function of temperature, it is possible to construct a temperature–concentration diagram as shown in Figure 36. This diagram assumes $\chi_s = 0.2$ and should be reasonably accurate for PS in CH and probably is fairly close for PS in cyclopentane as well.

The marginal regime (III) is found only in stiff polymer chains. Figure 37 shows the T–C diagram appropriate to a highly flexible chain such as PDMS where $n = C_\infty/6 = 1.0$. For $n \leqq 1$ region III is small and crossover may occur directly from good-solvent scaling behavior to theta behavior. Such a crossover is consistent with the PDMS data in Figure 30, where a distinct transition to higher slope is observed near $\tilde{\phi} \simeq \phi^{\dagger\dagger} = 0.1$.

Other Systems. Conflicting data and/or interpretations exist for cooperative diffusion of PS in BZ and THF. In BZ, for example, Adam and Delsanti[25] and Munch *et al.*[90] report exponents consistent with scaling laws, whereas Schaefer[61] finds an exponent of 0.5 consistent with marginal behavior. Similar discrepancies exist for PS in THF.

Figure 38 shows existing data for PS in BZ. These data can be fitted nicely with the scaling exponent of 0.75, confirming the observation of Adam and Delsanti[25] and Munch *et al.*[90] Scaling behavior at these high concentrations, however, is inconsistent with the T–C diagram in Figure 35 and also conflicts with viscosity[94] and sedimentation data.[75] The sedimentation data, in particular, are consistent with $\phi^\dagger \simeq 0.03$. In other words, it appears that most of the data in Figure 38 are in the crossover region between marginal and theta power laws as evidenced by the upward curvature of the data and the limiting slopes shown on the figure. The apparent exponent near 0.75 is a consequence of an attempt to fit the data in a crossover region and is not necessarily indicative of scaling.

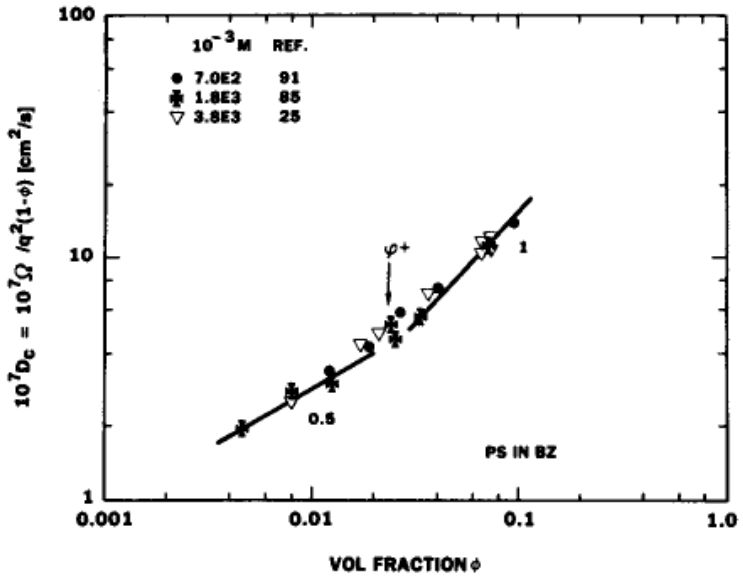

Figure 38. Collective diffusion constant for PS in benzene. The limiting slopes of 0.5 and 1.0 suggest that BZ is a marginal solvent. $T = 20°C$. The data of Reference 85 were taken at 25°C and reduced to 20°C assuming $D_c \sim T/\eta$.

The PS/THF system has been studied by at least four groups with different results and conclusions. Figure 39 shows the data of Schaefer *et al.*,[22] Mandema *et al.*,[23] and Amis and Han.[84] Although the scatter is substantial below $\phi = 0.05$, the data seem to follow power law behavior with a slope of ~ 0.6. From Table 1, this system should show scaling behavior below $\tilde{\phi} \simeq 0.05$ so we attribute the intermediate exponent to mean that the data are in the region-I–region-II crossover. The data of Yu *et al.*[68] are

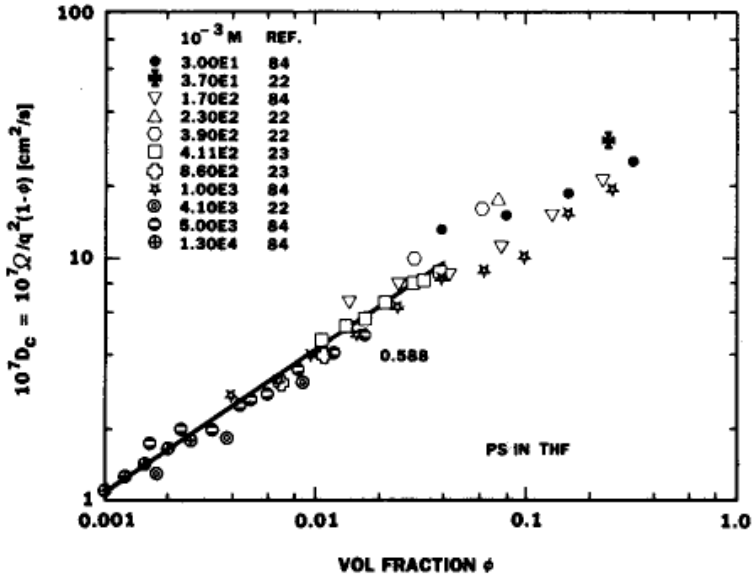

Figure 39. Collective diffusion constant for PS in tetrahedrofuran (THF) at 25°C.

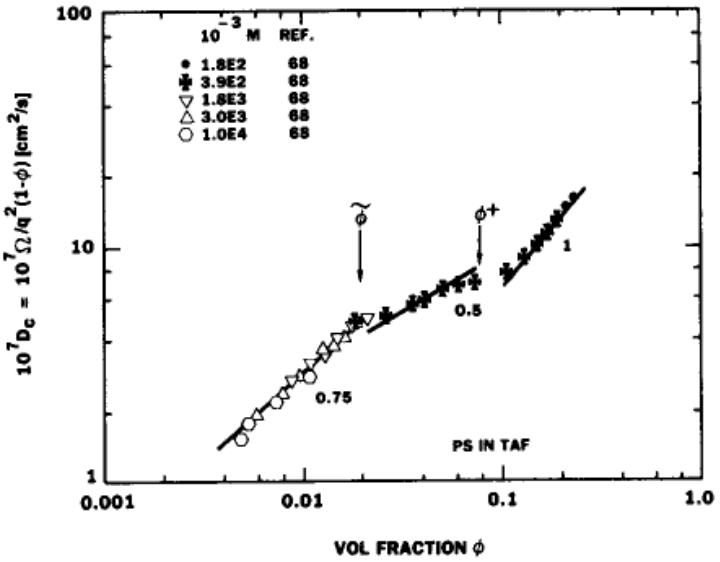

Figure 40. Collective diffusion constant of PS in THF measured at 30°C and reduced to 25°C. These are the only data that show two distinct transitions. The theory outlined here implies that the slope should be 0.5 between $\tilde{\phi}$ and $\phi^\dagger$. The data, however, show a substantially smaller slope.

not numerically consistent with Figure 39, but these data do show the expected crossovers. These data are plotted in Figure 40 where the ordinate is reduced to 25°C assuming $D_c \sim T/\eta$. These data show scaling below $\phi = 0.02$ and a thetalike power law above $\phi = 0.1$. In the marginal regime between 0.02 and 0.1, however, the power law exponent appears to be smaller than 0.5. It seems that in spite of the abundance of data, the PS/THF system is not well understood.

Table 4 tabulates the various crossovers both inferred from the model presented here and from the experimental data. Although some of the

Table 4. Crossover Points

	$\tilde{\phi}$		$\phi^\dagger$	
System	Equation (68)	Observed	Equation (79)	Observed
PS in				
EA	0.002	—	0.04	0.08
MEK	0.004	(0.004)	0.08	—
BZ	0.004	—	0.1	0.03
THF	0.01	0.02	0.2	0.1
TOL	0.02	0.07	0.3	0.2
PDMS in				
TOL	—	—	0.1	0.1

observed crossovers differ from the predicted values by as much as a factor of 5, there is a reasonably consistent trend with solvent quality. In view of the simplicity of the model used, even accuracy within a factor of 5 is encouraging.

5.4.2.3. Reptation: $qR_g \lesssim 1$. As q is decreased, one probes concentration fluctuations of longer Fourier spatial wavelength. Eventually, the condition is approached where the collective relaxation time $(D_c q^2)^{-1}$ becomes comparable to the reptation time T_R. At this point, reptation becomes the dominant relaxation mechanism and Ω is expected to reflect the chain self-diffusion constant D_s. Both T_R and D_t can be found from the simple reptation model described above.

The reptation time and self-diffusion constant can be obtained by a model based on one-dimensional diffusion of blobs in a tube.[4] That is, a polymer is pictured as a Rouse chain of renormalized monomers (blobs) of radius ξ_t, where the Rouse monomer radius or tube radius ξ_t is determined by the space-filling condition:

$$\rho = \frac{g_t}{\xi_t^3} \tag{80}$$

Here g_t is the number of monomers in a "tube blob." Equation (80) coupled with the appropriate chain statistics

$$\xi_t \sim g_t^{\nu} a, \qquad \tfrac{1}{2} < \nu < \tfrac{3}{5} \tag{81}$$

yields the tube radius as listed in Table 3 for the various concentration regimes described above. Note that in marginal systems the tube radius is not proportional to $\xi_\rho \sim \xi_2$. The multiplicity of length scales in marginal systems has led to considerable confusion in the interpretation of experiments which are sensitive to reptation. The model proposed here is not without conceptual problems, so reptation in marginal systems should still be considered an open question. In good solvents problems do not arise since all lengths (ξ_ρ, ξ_2, ξ_t) have the same concentration dependence.

The friction constant associated with the Rouse blobs in the tube is not necessarily proportional to ξ_t^{-1} because screening tells us that monomers are hydrodynamically coupled over distances comparable to the range ξ_ρ of the pair correlation function, not the tube radius ξ_t. Therefore, the friction constant of a tube blob ζ is

$$\zeta \sim 6\pi\eta\xi_\rho \tag{82}$$

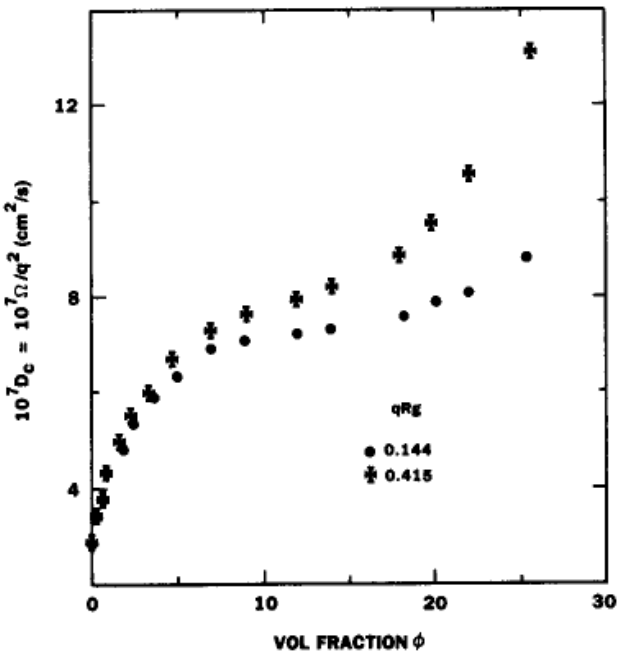

Figure 41. Concentration dependence of the initial slope of $S(q, t)$ for two values of qR_g.[68] For $qR_g \ll 1$ the mean relaxation rate is substantially reduced due to a reptation-type diffusion process. For $qR_g \ll 1$, collective diffusion is not possible.

Using $D_1 = g_\rho kT/N\zeta$ it is possible to calculate the time for the chain to escape its tube by *one-dimensional* diffusion[10]

$$T_R \sim \frac{(\text{tube length})^2}{D_1} \sim \frac{N^3 \xi_\rho \xi_t^2 \eta}{g_t^2 g_\rho kT}, \qquad \varphi \ll 1 \tag{83}$$

The reptation time calculated by equation (83) is listed in Table 3.

The crossover point for transition from cooperative diffusion to reptation can be found by equating the cooperative relaxation time $(D_c q^2)^{-1}$ with T_R, with the final result

$$q^2 R_g^2 = \left(\frac{\rho^*}{\rho}\right)^{9/4} \tag{84}$$

in good solvents. For $q^2 R_g^2 < (\rho^*/\rho)^{9/4}$, reptation is the dominant relaxation process. In marginal and theta systems, equation (84) is slightly modified $[q^2 R_g^2 = 0.44(\rho^*/\rho)^3]$.

The data of Yu *et al.*[68] shown in Figure 41 illustrate the transition to slower reptation dynamics at small q. These data show that as concentration increases, the correlation function is increasingly dominated by a slow relaxation process when $qR_g \ll 1$. The strong q dependence of Ω/q^2 at high concentration may explain the discrepancies in values of D_c reported by different groups working on the same system such as the PS/THF system described above.

The form of $S(q, t)$ in the reptation regime can be obtained[67] by evaluating equation (55) for $q\xi_\rho \ll 1$, $qR_g \ll 1$

$$S(q, t) = \rho g_\rho \left\{ \exp[-q^2(D_s + D_c)(1 - \phi)t] + \left[\left(\frac{N}{g_\rho}\right) - 1\right] \exp[-q^2 D_s(1 - \phi)t] \right\} \quad (85)$$

where we have assumed that the chain center of mass relaxes by self diffusion, D_s being the three-dimensional self-diffusion constant. Equation (85) predicts a bimodal decay, and this fact accounts for the nonexponential correlation functions which are generally reported in a semidilute solution.[61] In cross-linked gels, by contrast, the second term of equation (85) is absent and the observed correlation functions are exponential.

The amplitude A of the collective and self terms in equation (85) shows that

$$\frac{A_s}{A_c} = \left(\frac{N}{g_\rho}\right) - 1 \cong \left(\frac{\rho}{\rho^*}\right)^y, \qquad \begin{array}{ll} y = 5/4 & \text{(good)} \\ y = 1 & \text{(marginal)} \\ y = 2 & \text{(theta)} \end{array} \quad (86)$$

In other words, reptative self-diffusion becomes more important at high concentration. This behavior is seen not only in Figure 41 but also in the bimodal correlation functions of Jamieson *et al.*[81] shown in Figure 42. Here a slow relaxation process becomes increasingly important at high concentration for $qR_g < 1$.

In the limit $qR_g \ll 1$ or $t \gg (D_c q^2)^{-1}$, equation (85) simplifies to

$$S(q, t) \cong \rho N \exp[-q^2 D_s(1 - \phi)t] \quad (87)$$

This equation implies that the reptative diffusion constant D_t can be measured by PCS. The concentration dependence of the relaxation rate $\Gamma = D_s q^2(1 - \phi)$ can be obtained through the tube model. That is, since a time T_R is required for the chain to escape its tube whose trajectory is of dimension R_t

$$D_s \sim \frac{R_t^2}{T_R} = \left[\left(\frac{N}{g_t}\right)^{1/2} \xi_t\right]^2 T_R^{-1} \quad (88a)$$

$$\sim kTN^{-2} g_t g_\rho \xi_\rho^{-1} \eta^{-1}, \qquad \varphi \ll 1 \quad (88b)$$

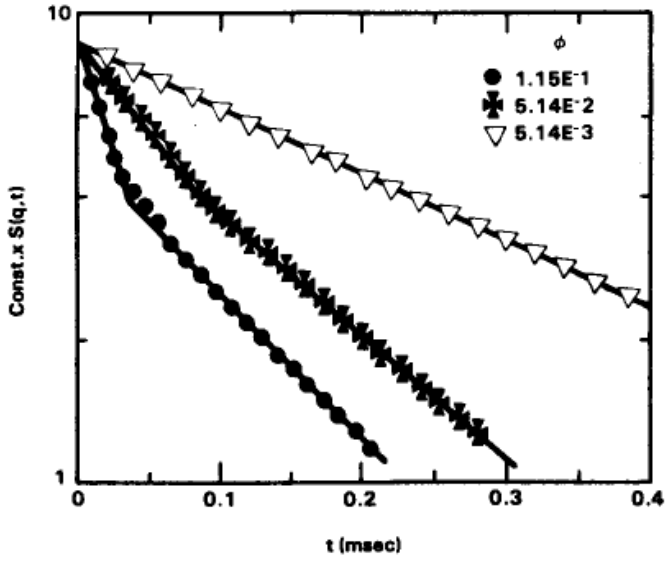

Figure 42. Measured correlation function for PS in THF at three concentrations.[81] At high concentration $S(q, t)$ is bimodal, reflecting both a collective and reptation relaxation mode. The data are for $M = 3.9 \times 10^5$ at 30°C. The upper curve is in the dilute regime.

The concentration dependence obtained from equation (88b) is listed in Table 3. For convenience, other quantities[4] are also listed, such as the elastic modulus E_{gel} and the viscosity $\eta_r = E_{gel} T_R$ and the sedimentation coefficient $s = g_\rho \xi_\rho^{-1}$.

Very little experimental work has been reported on the slowly decaying translational mode in semidilute solution, although forced Rayleigh scattering has been reported.[62] Amis and Han,[84] however, have studied this mode for PS in THF, and their data are shown in Figure 43. Here $N^2\Gamma/q^2(1-\phi)$ is plotted vs. volume fraction ϕ and lines are drawn with the appropriate slopes for good marginal and theta behavior. In the figure, Γ is the relaxation rate of $S(q, t)$ for $t \gg (D_c q^2)^{-1}$. $N^2\Gamma/q^2(1-\phi)$ should equal D_s in equation (88) if the model used here is correct. Here $(1-\phi)$ is a backflow correction. The data are reasonably consistent with equation (88b) with the crossover $\tilde{\phi}$ occurring at 0.01, which is close to $\tilde{\phi} \cong 0.02$ found in Figure 40 for the same system. At the highest concentrations, the curve drops precipitously and is not consistent with the ϕ^{-3} behavior predicted above $\phi^\dagger$. It must be realized that the precision of the data is poor for these very long correlation times, so ϕ^{-3} behavior is not necessarily out of the question. These data are also at the upper limit of semidilute solutions and very likely interchain interactions limit the validity of the friction constants used.

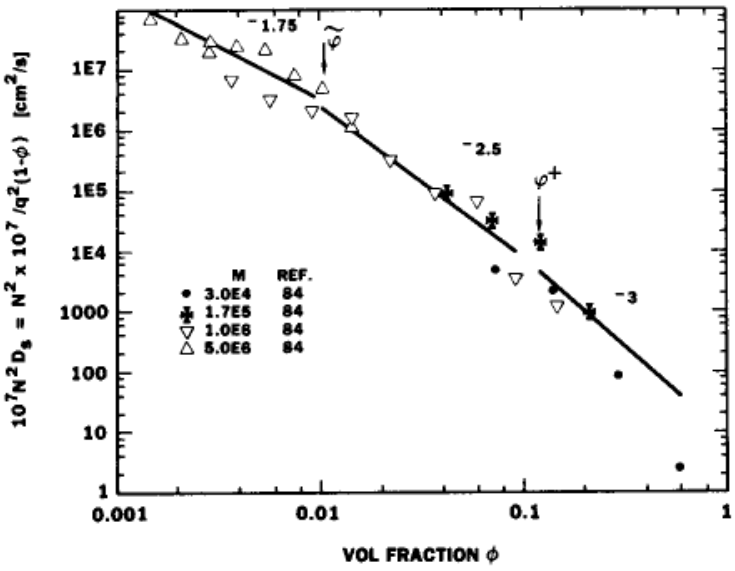

Figure 43. Self-diffusion constant taken from the measured relaxation rate Γ of the slowly decaying mode of $S(q, t)$. The ordinate should be $N^2 D_s$ and should follow the power laws indicated by the lines in the figure.

5.4.3. Conclusions

In this discussion of semidilute systems we have attempted to develop a framework that is useful to understand a large body of data that appear contradictory. In many cases, our interpretation conflicts with that of the experimenters themselves. Unfortunately, we have been forced, because of space limitations, to ignore these credible alternative interpretations. The model presented here, however, makes a broad range of predictions which have been subject to only limited experimental study.

It is interesting to note that in this entire review the concept of an "entanglement" has been completely ignored. Although entanglements may be important to certain viscoelastic properties, there is no evidence as yet that they play a significant role in $S(q, t, \rho)$ in the domains easily accessible to PCS measurements.

If rubberlike elasticity due to entanglements were playing a role in $S(q, t)$, then D_c would be proportional to E_{gel} rather than E_0.[63] In good and marginal solvents $E_{gel} \sim E_0$, so the observed concentration dependence of Ω would not change. In theta solvents ($T = \Theta$ not $\phi > \phi^\dagger$), however, D_c would be concentration independent in contradiction to Figure 33. Thus, based on limited data available, entanglements do not seem to affect cooperative diffusion.

If entanglements played a significant role in the reptation process, then D_s should show a dependence on N to a power larger than 2 and should also display a distinct change in behavior below the critical molecular

weight for entanglements.[66] To our knowledge, neither expectation is realized. Recent experiments by Selser[78] and theory by Ronca[79] do suggest that the detailed shape and q dependence of $S(q, t)$ reflect entanglements. This effect, however, appears as a small quartic term in the reptation part of $S(q, t)$. It appears, then, that although the broad features of semidilute dynamics do not reflect entanglements, undoubtedly they will be necessary to explain increasingly detailed aspects of polymers at high concentration.

REFERENCES

1. P. J. Flory, *Statistical Mechanics of Chain Molecules*, Interscience, New York (1969).
2. C. Croxton, *Introduction to Liquid State Physics*, Wiley, New York (1975).
3. P. J. Flory, *Principles of Polymer Chemistry*, Cornell University, Ithaca, New York (1953), Chap. 14.
4. P. G. de Gennes, *Scaling Concepts in Polymer Physics*, Cornell University, Ithaca, New York (1979).
5. H. Yamakawa, *Modern Theory of Polymer Solutions*, Harper and Row, New York (1971).
6. P. J. Flory, *Discuss. Faraday Soc.* **49**, 7 (1970).
7. Reference 2, Chap. 2.
8. B. Farnoux, F. Boue, J. P. Cotton, M. Daoud, G. Jannink, M. Nierlich, and P. G. de Gennes, *J. Phys. (Paris)* **39**, 77 (1978).
9. Reference 4, Chap. 6.
10. J. Kirkwood and J. Riseman, *J. Chem. Phys.* **16**, 565 (1948).
11. B. Zimm, *J. Chem. Phys.* **24**, 269 (1956).
12. P. G. de Gennes, *Macromolecules* **9**, 587, 594 (1976).
13. L. K. Nicholson, J. S. Higgins, and J. B. Hayter, *Macromolecules* **14**, 836 (1981).
14. T. A. King, A. Knox, W. I. Lee, and J. D. G. McAdam, *Polymer* **14**, 151 (1973).
15. J. des Cloizeaux and G. Weill, *J. Phys. (Paris)* **40**, 99 (1979).
16. A. Z. Akcasu and C. C. Han, *Macromolecules* **12**, 276 (1979).
17. D. W. Schaefer and J. G. Curro, *Ferroelectrics* **30**, 49 (1980).
18. J. G. Curro and D. W. Schaefer, *Macromolecules* **13**, 1199 (1980).
19. M. Benmouna and A. Z. Akcasu, *Macromolecules* **11**, 1187, 1193 (1978).
20. A. Z. Akcasu, M. Benmouna, and C. C. Han, *Polymer* **21**, 866 (1980).
21. (a) T. A. King, A. Knox, and J. D. G. McAdam, *Polymer* **14**, 293 (1973); (b) N. C. Ford, F. E. Karaz, and J. E. M. Owen, *Discuss. Faraday Soc.* **49**, 228 (1970).
22. D. W. Schaefer, J. F. Joanny, and P. Pincus, *Macromolecules* **13**, 1280 (1980).
23. W. Mandema and Z. Zeldenrust, *Polymer* **18**, 835 (1977).
24. P. N. Pusey, J. M. Vaughn, and V. G. Williams, *J. Chem. Soc., Trans. II* **70**, 1696 (1974).
25. M. Adam and M. Delsanti, *Macromolecules* **10**, 1229 (1977).
26. *Polymer Handbook*, 2nd Ed., J. Brandrup and E. H. Immergut, eds., Interscience, New York (1975).
27. J. Selser, *Macromolecules* **14**, 346 (1981).
28. S. Saeki, S. Konno, N. Kuwahara, M. Nakata, and M. Kaneko, *Macromolecules* **7**, 521 (1974).
29. R. Pecora, *J. Chem. Phys.* **43**, 1562 (1965).
30. P. G. de Gennes, *Physics*, **3**, 37 (1967).
31. E. Dubois-Violette and P. G. de Gennes, *Physics* **3**, 181 (1967).

32. R. Zwanzig, *J. Chem. Phys.* **60**, 2717 (1974).
33. (a) M. Fixman, *J. Chem. Phys.* **42**, 3831 (1965); (b) C. W. Pyun and M. Fixman, *J. Chem. Phys.* **42**, 3838 (1965).
34. A. Z. Akcasu and H. Gurol, *J. Polym. Sci., Polym. Phys. Ed.* **14**, 1 (1976).
35. J. des Cloizeaux, CEN (Saclay) Reports (1976).
36. J. Riseman and J. G. Kirkwood, in *Rheology, Theory and Applications*, F. R. Eirich, ed., Adademic Press, New York (1956).
37. P. E. Rouse, Jr., *J. Chem. Phys.* **21**, 1272 (1953).
38. J. E. Shore and R. Zwanzig, *J. Chem. Phys.* **63**, 5445 (1975).
39. R. Bellman, *Introduction to Matrix Analysis*, 2nd Ed., McGraw-Hill, New York (1970).
40. W. Burchard and M. Schmidt, *Polymer* **21**, 745 (1980).
41. A. Z. Akcasu and J. S. Higgins, *J. Polym. Sci. (Polym. Phys. Ed.)* **15**, 1745 (1977).
42. M. Benmouna, A. Z. Akcasu, and M. Daoud, *Macromolecules* **13**, 1703 (1980).
43. A. Perico, P. Piaggio, and C. Cuniberti, *J. Chem. Phys.* **62**, 2690 (1975).
44. M. Schmidt and W. Stockmayer (private communication).
45. G. Pouyet, J. Francois, J. Dayantis, and G. Weill, *Macromolecules* **13**, 176 (1980).
46. R. Zwanzig *et al.*, *Proc. Nat. Acad. Sci. USA* **60**, 381 (1981).
47. R. Ullman, *Macromolecules* **7**, 300 (1974).
48. J. T. Fong and A. Peterlin, *J. Res. Nat. Bur. Stand. Sect. B, Math. Sci.* **80B**, 273 (1976).
49. C. C. Han and A. Z. Akcasu, *Macromolecules* **14**, 1080 (1981).
50. M. Adam, M. Delsanti, and G. Pouyet, *J. Phys. Lett. (Paris)* **40**, L-435 (1979).
51. M. Daoud, thesis, Universite de Paris (1977).
52. H. Yamakawa, *J. Chem. Phys.* **36**, 2995 (1962).
53. S. Imai, *J. Chem. Phys.* **50**, 2116 (1969).
54. C. W. Pyun and M. Fixman, *J. Chem. Phys.* **41**, 957 (1964).
55. A. R. Altenberger and J. M. Deutch, *J. Chem. Phys.* **59**, 894 (1973).
56. A. Z. Akcasu and M. Benmouna, *Macromolecules* **11**, 1193 (1978).
57. A. Z. Akcasu, *Polymer* **22**, 1169 (1981).
58. C. C. Han and A. Z. Akcasu, *Polymer* **22**, 1165 (1981).
59. K. F. Freed and S. F. Edwards, *J. Chem. Phys.* **61**, 1189, 3626 (1974).
60. G. D. Patterson, J. R. Stevens, G. R. Alms, and C. P. Lindsey, *Macromolecules* **12**, 661 (1979).
61. D. W. Schaefer, *Polym. Prepr.* **19**, 452 (1978).
62. H. Hervet, L. Leger, and F. Rondelez, *Phys. Rev. Lett.* **42**, 1681 (1979).
63. F. Brouchard and P. G. de Gennes, *Macromolecules* **10**, 1157 (1977).
64. D. W. Schaefer, *Polym. Prepr.* **19**, 733 (1978).
65. E. Geissler and A. M. Hecht, *J. Phys. Lett. (Paris)* **40**, L-173 (1979).
66. J. Klein, *Macromolecules* **11**, 852 (1978).
67. E. J. Amis, C. C. Han, and Y. Matsushita, *Polymer* **25**, 650 (1984).
68. T. L. Yu, H. Reihanian, and A. M. Jamieson, *Macromolecules* **13**, 1590 (1980).
69. J. S. Higgins, L. K. Nicholson, and J. B. Hayter, *Polym. Prepr.* **22**, 86 (1981).
70. I. Noda, N. Kato, T. Kitano, and M. Nagasawa, *Macromolecules* **14**, 668 (1981).
71. C. E. H. Bawn, R. F. J. Freeman, and A. R. Kamaliddin, *Trans. Faraday Soc.* **46**, 677 (1950).
72. T. Tanaka, L. O. Hocker, and G. B. Benedek, *J. Chem. Phys.* **59**, 5151 (1973).
73. M. Daoud, J. P. Cotton, B. Farnoux, G. Jannink, G. Sarma, H. Benoit, R. Duplessix, R. Picot, and P. G. de Gennes, *Macromolecules* **8**, 804 (1975).
74. A. R. Khokhlov, *Polym. Sci. USSR* **20**, 3087 (1978).
75. B. Nyström and J. Roots, *J. Macromol. Sci. Rev. Macromol. Chem.* **C19**, 35 (1980).
76. M. A. Moore, *J. Phys. (Paris)* **38**, 265 (1977).

77. K. Okano, E. Wada, K. Kurita, and H. Fukuro, *J. Appl. Crystallogr.* **11**, 507 (1978).
78. J. Selser, *J. Chem. Phys.* **79**, 1044 (1983).
79. G. Ronca, to be published.
80. M. Daoud and G. Jannink, *J. Phys.* (*Paris*) **37**, 973 (1976).
81. A. M. Jamieson, H. Reihanian, J. G. Southwick, T. L. Yu and J. Blackwell, *Ferroelectrics* **30**, 267 (1980).
82. D. Richter, B. Ewen, and J. B. Hayter, *Phys. Rev. Lett.* **45**, 2121 (1980).
83. C. Reiss and H. Benoit, *C.R. Acad. Sci. Paris* **253**, 268 (1961).
84. E. J. Amis and C. C. Han, *Polymer* **23**, 1403 (1982).
85. D. W. Schaefer, unpublished.
86. B. Appelt and G. Meyerhoff, *Macromolecules* **13**, 657 (1980).
87. M. E. McDonnell and A. M. Jamieson, *J. Macromol. Sci. Phys.* **B13**, 67 (1977).
88. J. Roots and B. Nyström, *Macromolecules* **13**, 1595 (1980).
89. R. S. Chahal, W. P. Kao, and D. J. Patterson, *Chem. Soc., Faraday Trans.* **69**, 1834 (1973).
90. J. P. Munch, S. Candau, J. Hertz, and G. J. Hild, *J. Phys.* (*Paris*) **38**, 971 (1977).
91. J. Roots, B. Nyström, B. Porsch, and L. O. Sundelöf, *Polymer* **20**, 337 (1979).
92. J. P. Munch, P. L. Lemarichal, and S. Candau, *J. Phys.* (*Paris*) **38**, 1499 (1977).
93. P. Mathiez, C. Mouttet, and G. Weisbuch, *J. Phys.* (*Paris*) **41**, 519 (1980).
94. M. Adam and M. Delsanti, *Polymer. Prepr.* **22**, 104 (1981).
95. M. Daoud and G. Jannink, *J. Phys. Lett.* (*Paris*) **41**, L-217 (1980).